Multimodal MRI Marker of Cognition Explains the Association Between Cognition and Mental Health in UK Biobank

Running Title: MRI explains cognition-mental health relationship

Irina Buianova, MSc[1], Mateus Silvestrin, PhD[2,3], Jeremiah Deng, PhD[4], Narun Pat, PhD[1]

[1]Department of Psychology, University of Otago, Dunedin, New Zealand

[2]Federal University of the São Francisco Valley, Petrolina, Brazil

[3]National Institute of Social and Affective Neuroscience, Petrolina, Brazil

[4]School of Computing, University of Otago, Dunedin, New Zealand

Corresponding author:

Irina Buianova, MSc, Department of Psychology, University of Otago, William James Building, 275 Leith Walk, Dunedin 9016, New Zealand

Email: is.buyanova@gmail.com

Abstract

Background

Cognitive dysfunction often co-occurs with psychopathology. Advances in neuroimaging and machine learning have led to neural indicators that predict individual differences in cognition with reasonable performance. We examined whether these neural indicators explain the relationship between cognition and mental health in the UK Biobank cohort (n > 14000).

Methods

Using machine learning, we quantified the covariation between general cognition and 133 mental health indices and derived neural indicators of cognition from 72 neuroimaging phenotypes across diffusion-weighted MRI (dwMRI), resting-state functional MRI (rsMRI), and structural MRI (sMRI). With commonality analyses, we investigated how much of the cognition-mental health covariation is captured by each neural indicator and neural indicators combined within and across MRI modalities.

Results

The predictive association between mental health and cognition was at r=0.3. Neuroimaging phenotypes captured 2.1% to 25.8% of the cognition-mental health covariation. The highest proportion of variance explained by dwMRI was via the number of streamlines connecting cortical regions (19.3%), by rsMRI via functional connectivity between 55 large-scale networks (25.8%), and by sMRI via the volumetric characteristics of subcortical structures (21.8%). Combining neuroimaging phenotypes within modalities improved the explanation to 25.5% for dwMRI, 29.8% for rsMRI, and 31.6% for sMRI, and combining them across all MRI modalities enhanced the explanation to 48%.

Conclusions

We present an integrated approach to derive multimodal MRI markers of cognition that can be transdiagnostically linked to psychopathology showing that the predictive ability of neural indicators extends beyond the prediction of cognition itself, allowing us to capture the cognition-mental health covariation.

Keywords: cognition, mental health, magnetic resonance imaging, machine learning, UK Biobank, predictive modeling

3

Introduction

Cognition and mental health are closely intertwined [1]. Cognitive dysfunction is present in various mental illnesses including anxiety [2, 3], depression [4–6], and psychotic disorders [7–9]. In some cases, altered cognitive functioning is directly related to psychiatric symptom severity [10]. Furthermore, cognitive impairments in psychopathology are often stable and persist upon alleviation of psychiatric symptoms [11–13]. Twin studies estimate the heritability of the relationship between cognition and mental health to be around 25%-40% [14]. However, we still lack neural indicators that capture this relationship, which hinders its investigation at the neural level.

Recent efforts in brain Magnetic Resonance Imaging (MRI) and machine learning have led to predictive models that allow us to create MRI-based neural indicators of cognition with reasonable predictive performance [15–17]. These models are designed to predict cognition based on different cognitive tasks in unseen individuals who are not part of the modeling processes [18, 19]. Yet, the extent to which MRI-based neural indicators designed to predict cognition capture the same variance that mental health shares with cognition remains unknown. Demonstrating that MRI-based neural indicators of cognition capture the covariation between cognition and mental health will thereby support the utility of such indicators for understanding the etiology of mental health [20].

Different MRI modalities measure different aspects of the brain, and MRI quantification techniques capture different brain features, resulting in distinct neuroimaging phenotypes. This means there are numerous approaches to derive neural indicators of cognition from MRI data. For example, diffusion-weighted MRI (dwMRI) measures the shape and amount of water diffusion in various directions and tissue compartments [21]. Different dwMRI metrics, such as fractional anisotropy (FA) which quantifies the degree of water diffusion directionality, and the streamline count which indirectly reflects structural connectedness between the two regions (structural connectome), provide information about white matter orientation, density, and microstructural integrity [22–24]. Resting-state functional MRI (rsMRI) measures spontaneous low-frequency fluctuations in the

4

Blood Oxygenation Level Dependent (BOLD) signal in the absence of a task, enabling the investigation of resting-state functional connectivity (RSFC) [25]. RSFC from rsMRI can be estimated between pairs of parcellated grey matter regions (functional connectome) or between widespread networks derived from the Independent Component Analysis (ICA). Structural MRI (sMRI) uses T1-weighted and T2-weighted imaging to quantify various aspects of brain anatomy and morphology. For example, the morphology of the cerebral cortex and white matter can be quantified by measuring grey or white matter thickness, volume, and area in regions defined by different atlases, whereas the characteristics of subcortical regions are conventionally quantified with volumes of subcortical nuclei and their subdivisions [26, 27]. Previous studies using machine learning have shown that both the choice of MRI modality and quantification method within each modality affect the performance of MRI-based models in capturing cognition [15, 17, 28]. Dhamala and colleagues found that the predictive ability of structural and functional connectomes largely depends on the choice of atlases used to parcellate grey matter and how they were derived [28].

Given the heterogeneity of neuroimaging phenotypes from different MRI modalities, drawing information across them may boost the predictive ability of MRI-based neural indicators [29]. One way to integrate multiple neuroimaging phenotypes across MRI modalities is a stacking approach which uses two levels of machine learning. First, researchers build a predictive model from each neuroimaging phenotype (e.g., cortical thickness from different grey matter parcellations) to predict a target variable (e.g., cognition). Next, in the stacking level, they use predicted values (i.e., cognition predicted from each neuroimaging phenotype) from the first level as features to predict the target variable [15]. Previous studies show that integrating multimodal neuroimaging phenotypes into “stacked models” enhances the prediction of cognition [15–17, 30]. Here, we aim to determine whether this improvement extends beyond the prediction of cognition itself, allowing us to capture more covariation between cognition and mental health.

Using the largest population-level dataset, the UK Biobank, we investigated (a) which neuroimaging phenotypes yield a neural indicator of cognition that explains the relationship

between cognition and mental health the most and (b) whether combining neuroimaging phenotypes within and across MRI modalities enhances the explanation of this relationship. We started by deriving a general cognition factor or the *g*-factor from twelve cognitive scores from different tasks. The *g*-factor underlies variability across cognitive domains and reflects the overall cognition [31, 32]. Next, we applied machine learning to predict the *g*-factor from 133 mental health indices and 72 neuroimaging phenotypes in unseen participants. For neuroimaging, we created predictive models from both individual neuroimaging phenotypes and phenotypes combined within and across three MRI modalities via stacking. Finally, we conducted commonality analyses [33] to quantify the contribution of neural indicators of cognition based on different neuroimaging phenotypes to explaining the relationship between cognition and mental health.

Methods and Materials

Study Design and Participants

We used cognition, mental health, and MRI data collected at the first imaging visit (2014-2019) and additional mental health data collected online from the UK Biobank (UK Biobank Resource Application 70132), a prospective epidemiological study involving individuals aged 40 to 69 years at recruitment. The analyses included participants who had all brain MRI scans, performed all cognitive tests, and completed full mental health questionnaires (Table 1).

Table 1. The number, age, and sex of participants who completed all cognitive tests, mental health questionnaires, and MRI scanning

	N participants	Age: mean (SD) years	Age: Range	% Females
Cognitive Tests	31 614	64.51 (7.66)	46.0–83.0	51.35%
Mental Health Questionnaire	21 077	64.63 (7.63)	47.0–82.0	53.0%
Cognitive Tests, Mental Health	17 250	64.25 (7.53)	47.0–82.0	54.68%

6

Questionnaire, and dwMRI				
Cognitive Tests, Mental Health Questionnaire, and rsMRI	17 005	64.2 (7.52)	47.0–82.0	54.92%
Cognitive Tests, Mental Health Questionnaire, and sMRI	14 793	64.21 (7.56)	47.0–82.0	54.62%
Cognitive Tests, Mental Health Questionnaire, and all MRI	14 256	64.04 (7.49)	47.0–82.0	54.97%

Cognition

To derive the *g*-factor, we used twelve scores from eleven cognitive tests (Fig. 1 and Supplementary Tables 1–3) [34]. A detailed description of cognitive tasks is provided in the UK Biobank showcase (http://biobank.ndph.ox.ac.uk/showcase/label.cgi?id=100026) and discussed elsewhere [34]. To capture overall variability in cognition, we built a *g*-factor hierarchical model using exploratory structural equation modeling (ESEM). Here, the *g*-factor underlies a set of latent factors which, in turn, underlies 12 cognitive scores (Fig. 1, 2 and Supplementary Materials, S1).

Mental Health

Mental health measures encompassed 133 variables from twelve groups: mental distress, depression, clinical diagnoses related to the nervous system and mental health, mania (including bipolar disorder), neuroticism, anxiety, addictions, alcohol and cannabis use, unusual/psychotic experiences, traumatic events, self-harm behaviours, and happiness and subjective well-being (Fig. 1 and Supplementary Tables 4 and 5). We used self-report questionnaires collected from all participants and composite diagnostic scores computed according to Davis et. al and Dutt et al. [35, 36]. We explain how we derive mental health scores in Supplementary Materials (S2).

Neuroimaging

For MRI-based models, we used dwMRI, rsMRI, and sMRI (Fig. 1 and Supplementary Table 6). MRI acquisition protocols are available at http://biobank.ctsu.ox.ac.uk/crystal/refer.cgi?id=2367. MRI processing pipelines are described in the UK Biobank brain imaging documentation (https://biobank.ctsu.ox.ac.uk/crystal/crystal/docs/brain_mri.pdf) and discussed elsewhere (Supplementary Materials, S3) [37, 38].

MRI data processed by the UK Biobank are available as imaging-derived phenotypes (IDPs). In addition to UK Biobank's IDPs, we used structural connectomes and BOLD time series created by Mansour and colleagues [39]. We used structural connectomes for six combinations of cortical and subcortical atlases: the Desikan-Killiany (aparc) cortical atlas [40] + Melbourne Subcortical Atlas scale I (MSA-I) [41], the Destrieux (aparc.a2009s) cortical atlas [42] + MSA-I [41], the Glasser cortical atlas [43] + MSA-I [41], the Glasser cortical atlas [43] + MSA-IV [41], the Schaefer atlas for 200 cortical regions (7 networks) [44, 45] + MSA-I [42], and the Schaefer atlas for 500 cortical regions (7 networks) [44, 45] + MSA-IV [41]. Since the BOLD time series data were provided separately for cortical and subcortical parcellations, we combined them according to the combinations used for structural connectomes (Supplementary Table 6).

dwMRI

To quantify dwMRI, we used 42 neuroimaging phenotypes. dwMRI IDPs included FA, diffusion tensor mode (MO), mean diffusivity (MD), and three eigenvalues of the diffusion tensor (L1, L2, L3) derived from diffusion tensor fitting, as well as intracellular volume fraction (ICVF), isotropic or free water volume fraction (ISOVF), and the orientation dispersion index (OD) from NODDI (Neurite Orientation Dispersion and Density Imaging) for 48 and 27 white matter tracts reconstructed with tract-based spatial statistics (TBSS) and probabilistic tractography, respectively [46–51]. Structural connectome data included matrices with quantitative metrics for each node pair from six atlas combinations. The metrics included streamline count, fibre bundle capacity (from

Spherical-Deconvolution Informed Filtering of Tractograms, SIFT2), mean streamline length, and mean FA (Supplementary Table 6) [39].

rsMRI

To quantify rsMRI, we leveraged 10 neuroimaging phenotypes. rsMRI IDPs included functional connectivity metrics – normalized temporal and partial temporal correlations between nodes' time series – and network amplitudes (the standard deviations of network time series [52]) for 21 and 55 networks (Independent Components, ICs) from ICA applied at 25 and 100 dimensions. We also applied tangent space parameterization to 21 and 55 networks to derive an additional metric for RSFC. Tangent space parameterization matrices were computed as deviations of subjects' connectivities from the group connectivity matrix [53–55]. To obtain functional connectomes from the parcellated BOLD time series data, we calculated full and partial Pearson correlations for each node pair and applied tangent parameterization to six atlas combinations (Supplementary Table 6).

sMRI

To quantify sMRI, we used 20 neuroimaging phenotypes. sMRI IDPs from T1-weighted MRI included grey and white matter volumes and mean intensity, cortical area and thickness, the volume of subcortical structures and cerebrospinal fluid, grey/white matter contrast (fractional contrast between grey and white matter intensities), and total brain volume for eight segmentation strategies: regional grey matter volumes (FSL FAST) [56], subcortical volumes (FSL FIRST) [57], FreeSurfer automated subcortical volumetric segmentation (ASEG), FreeSurfer *ex-vivo* Brodmann Area Maps, FreeSurfer Destrieux (a2009s), FreeSurfer Desikan-Killiany-Tourville parcellation, FreeSurfer Desikan-Killiany parcellation (grey/white matter intensity, pial surface, and white matter surface), and subcortical volumetric subsegmentation (FreeSurfer's ASEG and Bayesian segmentation of hippocampal subregions) [58]. sMRI IDPs from T2-weighted MRI included the total volumes of deep white matter, periventricular white matter, and white matter hyperintensities (Supplementary Table 6).

9

We corrected each MRI modality for common and specific sets of MRI-related confounds described in detail in Alfaro-Almagro et al. (Supplementary Table 7) [59]. The procedure for confound modeling is discussed in Supplementary Materials (S4).

Data analysis

We used a nested cross-validation approach to build machine-learning models to predict cognition from mental health indices and neuroimaging phenotypes. First, we split data into five outer folds. In each outer fold, we allocated 80% of the data points to the outer-fold training set for model tuning and the remaining 20% to the outer-fold test set for model evaluation (Fig. 1). Within each outer-fold training set, we further divided the data into ten inner folds. We iteratively treated each of the ten inner folds as an inner-fold validation set, and the rest as the inner-fold training set. We used the inner-fold training set to perform hyperparameter tuning and select the best hyperparameters based on model performance in the inner-fold validation set. The best hyperparameters, as determined by the minimal mean squared error (*MSE*), were then used in the final models in the outer-fold test set. To evaluate overall predictive performance, we computed Pearson *r*, the coefficient of determination (R^2), the mean absolute error (*MAE*), and the *MSE* between the predicted *g*-factor based on mental health and neuroimaging phenotypes and the observed *g*-factor derived directly from 12 cognitive scores, in each outer-fold test set. To combine information from neuroimaging phenotypes within and across MRI modalities, we used values predicted from the outer-fold training sets as inputs for the stacked model. In each outer fold, we standardized the data within the train set and applied the mean and standard deviation to the corresponding test set before modeling the *g*-factor, before regressing modality-specific confounds from MRI data, and before stacking.

With mental health and neuroimaging phenotypes, we used Partial Least Squares Regression (PLSR) as the base model to predict the *g*-factor. For rsMRI neuroimaging phenotypes, we treated connectivity metrics (full correlation, partial correlation, and tangent space parametrization) as hyperparameters. To obtain predicted values from a tuned model, we selected a functional

connectivity metric with the highest performance in the training set (Supplementary Materials, S5). We then used stacking to combine neuroimaging phenotypes within and across MRI modalities. Specifically, we treated predicted values of the *g*-factor obtained in PLSR models based on neuroimaging phenotypes within each of the three MRI modalities as features, which resulted in stacked models based on each MRI modality: "dwMRI Stacked", "rsMRI Stacked", and "sMRI Stacked". Additionally, we fed values predicted from all neuroimaging phenotypes in a single model ("all MRI Stacked") (Fig. 1). We used four algorithms to train stacked models – ElasticNet, Random Forest, XGBoost, and Support Vector Regression, – choosing one from four algorithms each time (Supplementary Materials, S6). For further analyses (i.e., commonality analyses below), we used the *g*-factor predicted by the algorithm that resulted in the highest mean R^2. To evaluate the distribution of performance indices, we pooled predicted and observed values of the *g*-factor from each outer-fold test set and calculated a bootstrap distribution of Pearson *r* (Fig. 1). We performed bootstrapping by sampling randomly with replacement for 5000 times.

Finally, we conducted a commonality analysis to quantify how much of the cognition-mental health relationship is captured by MRI-based neural indicators [34]. We explain this analysis in detail in Supplementary Materials (S7). Briefly, we first combined observed *g*-factor (i.e., the values derived directly from cognitive scores, not mental health or MRI data) and predicted *g*-factor (i.e., the values predicted from either mental health indices or neuroimaging phenotypes) from all outer-fold test sets. We then applied a series of linear regression models where we treated the observed *g*-factor as a response variable and the predicted *g*-factor from mental health (mental health-*g*) and the predicted *g*-factor from neuroimaging phenotypes (neuroimaging-*g*) as two separate explanatory variables. We then decomposed the variance of the observed *g*-factor to the variance explained uniquely or commonly by mental health-*g* and neuroimaging-*g*. We quantified the contribution of each neuroimaging phenotype to explaining the cognition-mental health relationship by a percentage ratio between (a) the common effects between mental health-*g* and neuroimaging-*g* and (b) the total effects of mental health-*g*. That is, the nominator is the common variance that

neuroimaging-*g* shares with mental health-*g* in explaining the observed *g*-factor, whereas the denominator is the variance of mental health-*g* that explains the observed *g*-factor regardless of neuroimaging-*g*.

We also examined if the performance of neuroimaging phenotypes in predicting cognition *per se is* related to their ability to explain the link between cognition and mental health. Here we computed the correlation between the predictive performance of each neuroimaging phenotype and the proportion of the cognition-mental health relationship it captures. To understand how demographic factors, including age and sex, contribute to this relationship, we also conducted a separate set of commonality analyses treating age, sex, age^2, age×sex, and age^2×sex as an additional set of explanatory variables (Fig. 1).

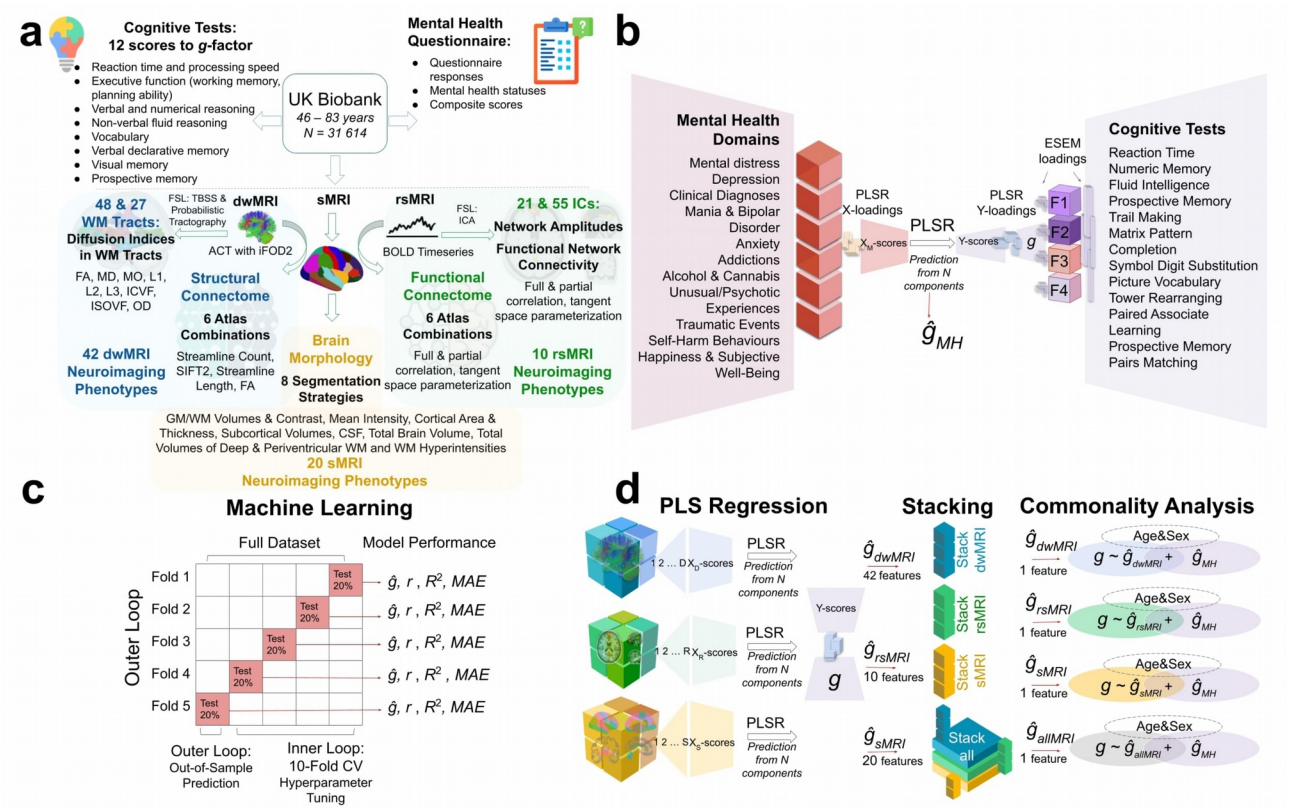

Figure 1. Experimental design. a UK Biobank variables: cognitive tests, mental health, and neuroimaging phenotypes from three MRI modalities. **b** Derivation of the *g*-factor from cognitive performance scores with Exploratory Structural Equation Modeling (ESEM) and prediction of the *g*-factor from mental health indices using Partial Least Squares Regression (PLSR). **c** Scheme of the machine learning model (PLSR) with nested cross-validation. **d** Scheme of the two-level predictive modeling and commonality analyses. First, individual neuroimaging phenotypes from dwMRI (42

12

phenotypes), rsMRI (10 phenotypes), and sMRI (20 phenotypes) are used as features to predict the *g*-factor. Then, *g*-factor values predicted from distinct neuroimaging phenotypes are combined within each modality ("Stack dwMRI", "Stack rsMRI", and "Stack sMRI") as well as across all modalities ("Stack all") and used as features, resulting in one predicted value per subject per stacked model ($\hat{g}_{dwMRI}$, $\hat{g}_{rsMRI}$, $\hat{g}_{sMRI}$, and $\hat{g}_{allMRI}$). Finally, values predicted fom MRI data together with the values predicted from mental health indices ($\hat{g}_{MH}$) are used as independent explanatory variables in commonality analyses. X_D*-scores*, X_R*-scores*, X_s*-scores*, and *Y-scores* weighted linear combinations of the original features (dwMRI, rsMRI, and sMRI neuroimaging phenotypes, respectively) in PLSR, *WM* white matter, *TBSS* tract-based spatial statistics, *ACT* anatomically-constrained tractography, *iFOD2* Fiber Orientation Distributions, *FA* fractional anisotropy, *MD* mean diffusivity, *MO* diffusion tensor mode, *L1*, *L2*, *L3* eigenvalues of the diffusion tensor, *ICVF* intracellular volume fraction, *OD* orientation dispersion index, *ISOVF* isotropic volume fraction, *BOLD* blood oxygenation level dependent signal, *ICA* independent component analysis, *GM* grey matter, *CSF* cerebrospinal fluid, *F1*, *F2*, *F3*, *F4* latent factors from ESEM, *ESEM loadings*, loadings of the test scores onto the latent factors and loadings of the latent factors onto the *g*-factor, *X-loadings* and *Y-loadings* loadings of the predictor (mental health measures, X) and target (*g*-factor, Y) variables, respectively, onto the PLSR components, X_M*-scores* and *Y-scores* the weighted linear combinations of the original predictor (mental health measures) and target (*g*-factor) variables, respectively, $\hat{g}_{MH}$ values of the *g*-factor predicted from mental health features, $\hat{g}$ predicted values of the *g*-factor, *r* Pearson *r* (between original and predicted values of the *g*-factor), R^2 coefficient of determination (between original and predicted values of the *g*-factor), *MAE* mean absolute error, *CV* cross-validation.

Results

Derivation of *g*-factor

In each fold, model performance estimates suggested good data factorability. According to parallel factor analysis, four factors were sufficient to explain the latent structure of the dataset (Fig. 2a). ESEM further supported the construct validity of factor structure (Fig. 2a). The *g*-factor captured around 39% of the variance in cognitive scores (Supplementary Materials, S8, Supplementary Tables 8–11).

Predictive Modeling

Mental health

13

On average, information about mental health predicted the *g*-factor at R^2_{mean} = 0.10 and r_{mean} = 0.31 (Fig. 2b and 2c and Supplementary Materials, S9, Supplementary Table 12).

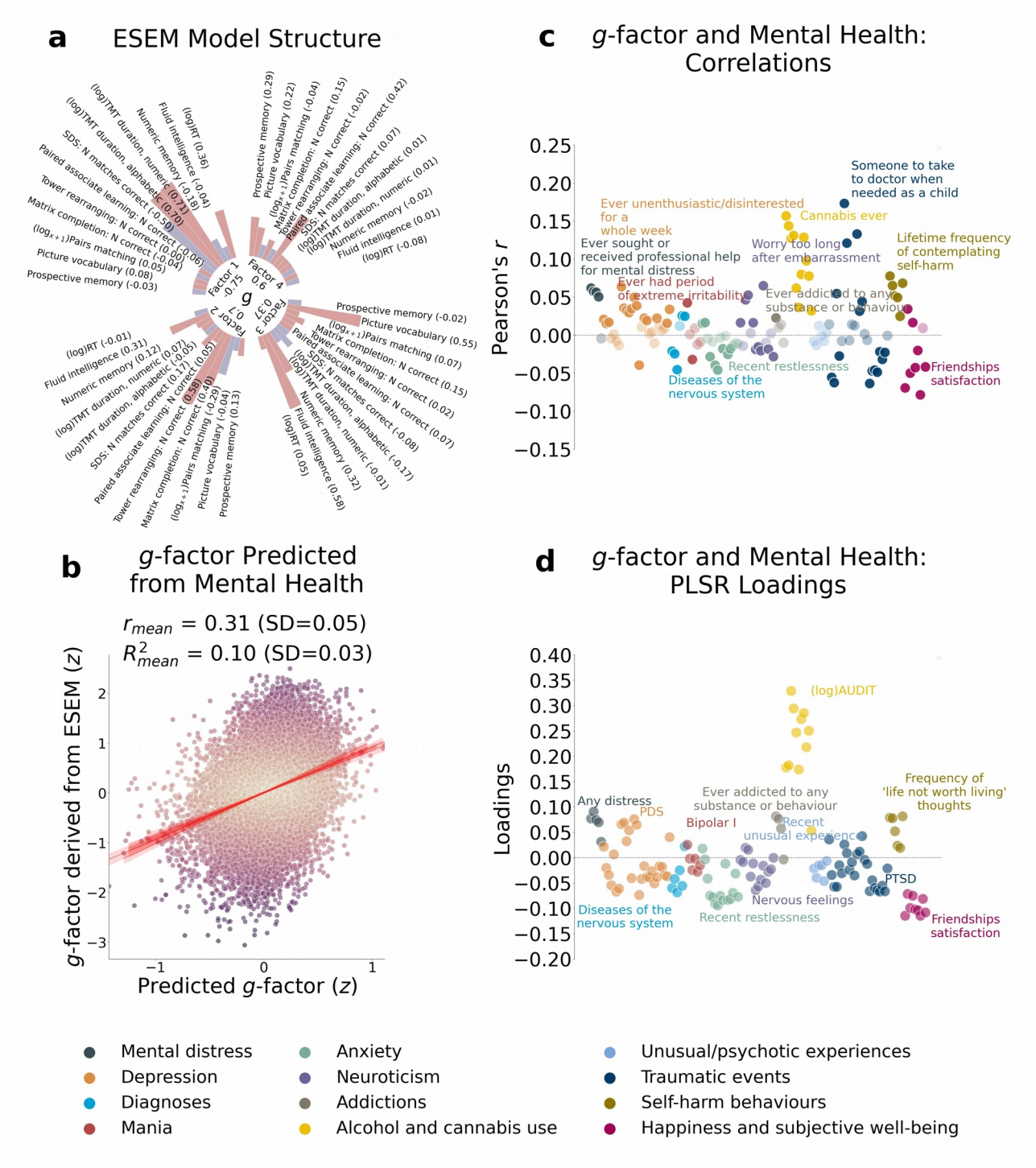

Figure 2. *g*-factor modeling and the relationship between the *g*-factor and mental health features. In our analysis, we derived the *g*-factor and built machine learning models in each outer fold separately. For visualization purposes, we

14

display the results of the (a) Exploratory Structural Equation Modeling (ESEM) performed on a sample of 31 614 participants and (b) Partial Least Squares Regression (PLSR) model for the *g*-factor and mental health built on a sample of 21 077 participants with a single train/test split (80%/20%) as representations of ESEM and PLSR model structures across five folds. **a** Loadings of the cognitive test scores onto four latent factors and loading of the latent factors onto the *g*-factor based on the ESEM. **b** Scatterplot of the observed *g*-factor and *g*-factor predicted from mental health indices with PLSR. Out-of-sample predictive performance of the PLSR model is evaluated with Pearson r and R^2 averaged across five folds. c Pearson correlations between the *g*-factor and mental health indices. Mental health features are grouped into categories. Within each category, a feature with the highest absolute value of Pearson r is annotated. Pale and bright dots represent non-significant and significant correlations, respectively. **d** Loadings of mental health indices in the PLSR model showing the relationships between the features (mental health) and the target variable (*g*-factor). The loadings are averaged across all PLSR components and weighted by R^2 in the train set. Mental health features are grouped into categories. Within each category, a feature with the highest absolute value of the loading is annotated. *SD* standard deviation.

MRI

The predictive performance of neuroimaging phenotypes varied from low to moderate. At the modality level, rsMRI and dwMRI showed the highest and lowest performance, respectively (Fig. 3b). On average, neuroimaging phenotypes stacked within dwMRI, rsMRI, and sMRI predicted the *g*-factor at R^2_{mean} = 0.073, 0.105, and 0.095, and r_{mean} = 0.27, 0.33, and 0.3, respectively. Stacking all 72 neuroimaging phenotypes boosted the predictive performance of the MRI-based model for cognition to R^2_{mean} = 0.159 and r_{mean} = 0.398 (Fig. 3a). The best algorithm for the stacked model was XGBoost. We outline results for each neuroimaging phenotype, each MRI modality, and each stacking algorithm in Supplementary Materials (S10).

dwMRI

Overall, models based on structural connectivity metrics performed better than TBSS and probabilistic tractography. TBSS, in turn, performed better than probabilistic tractography (Fig. 3b and Supplementary Table 13). The number of streamlines connecting each node pair in aparc MSA-I parcellation had the best predictive performance among all dwMRI neuroimaging phenotypes (R^2_{mean} = 0.052, r_{mean} = 0.227). The mean connectome length for nodes derived from the Schaefer

15

atlas for 500 cortical areas combined with MSA-IV had the lowest performance among all structural connectivity metrics (R^2_{mean} = 0.018, r_{mean} = 0.145; for bootstrapped Pearson *r* see Fig. 3b). Among dwMRI IDPs, eigenvalue L2 from TBSS had the best predictive performance (R^2_{mean} = 0.045, r_{mean} = 0.207), and MO and OD derived with probabilistic tractography were least predictive of the *g*-factor (R^2_{mean} = 0.006, r_{mean} = 0.076 and R^2_{mean} = 0.01, r_{mean} = 0.099, respectively).

Stacking *g*-factor values predicted from all dwMRI neuroimaging phenotypes improved the predictive performance of dwMRI to R^2_{mean} = 0.073 and r_{mean} = 0.265 (Fig. 3a). The best algorithm for the stacked model was Random Forest.

rsMRI

Among RSFC metrics for 55 and 21 ICs, tangent parameterization matrices yielded the highest performance in the training set compared to full and partial correlations as indicated by the cross-validation score. Among RSFC metrics for parcellated time series data, full correlation matrices performed best in the training set. Overall, RSFC between 55 ICs quantified with tangent space parameterization had the highest predictive performance (R^2_{mean} = 0.088, r_{mean} = 0.3) followed by RSFC between 200 cortical and 16 subcortical regions (Schaefer cortical atlas + MSA-I) measured with full correlation (R^2_{mean} = 0.07, r_{mean} = 0.27). The predictive performance of 21 and 55 ICs amplitudes was the lowest (R^2_{mean} = 0.013, r_{mean} = 0.14 and R^2_{mean} = 0.019, r_{mean} = 0.11, respectively; Fig. 3b and Supplementary Table 14).

Stacking *g*-factor values predicted from rsMRI neuroimaging phenotypes considerably improved the predictive performance of rsMRI to R^2_{mean} = 0.105 and r_{mean} = 0.325 (Fig. 3a and). Similar to dwMRI, the best algorithm in the stacked model was Random Forest.

sMRI

Subcortical volumetric subsegmentation and FreeSurfer subcortical volumetric segmentation (ASEG) had the highest performance among all sMRI neuroimaging phenotypes (R^2_{mean} = 0.068, r_{mean} = 0.244 and R^2_{mean} = 0.059, r_{mean} = 0.235, respectively). Grey matter morphological

characteristics from *ex-vivo* Brodmann Area Maps showed the lowest predictive performance (R^2_{mean} = 0.008, r_{mean} = 0.089; Fig. 3b and Supplementary Table 15).

Stacking *g*-factor values predicted from all sMRI neuroimaging phenotypes improved the model's predictive performance to R^2_{mean} = 0.095 and r_{mean} = 0.298. The best algorithm in the stacked model was Support Vector Regression (Fig. 3a and Supplementary Table 16).

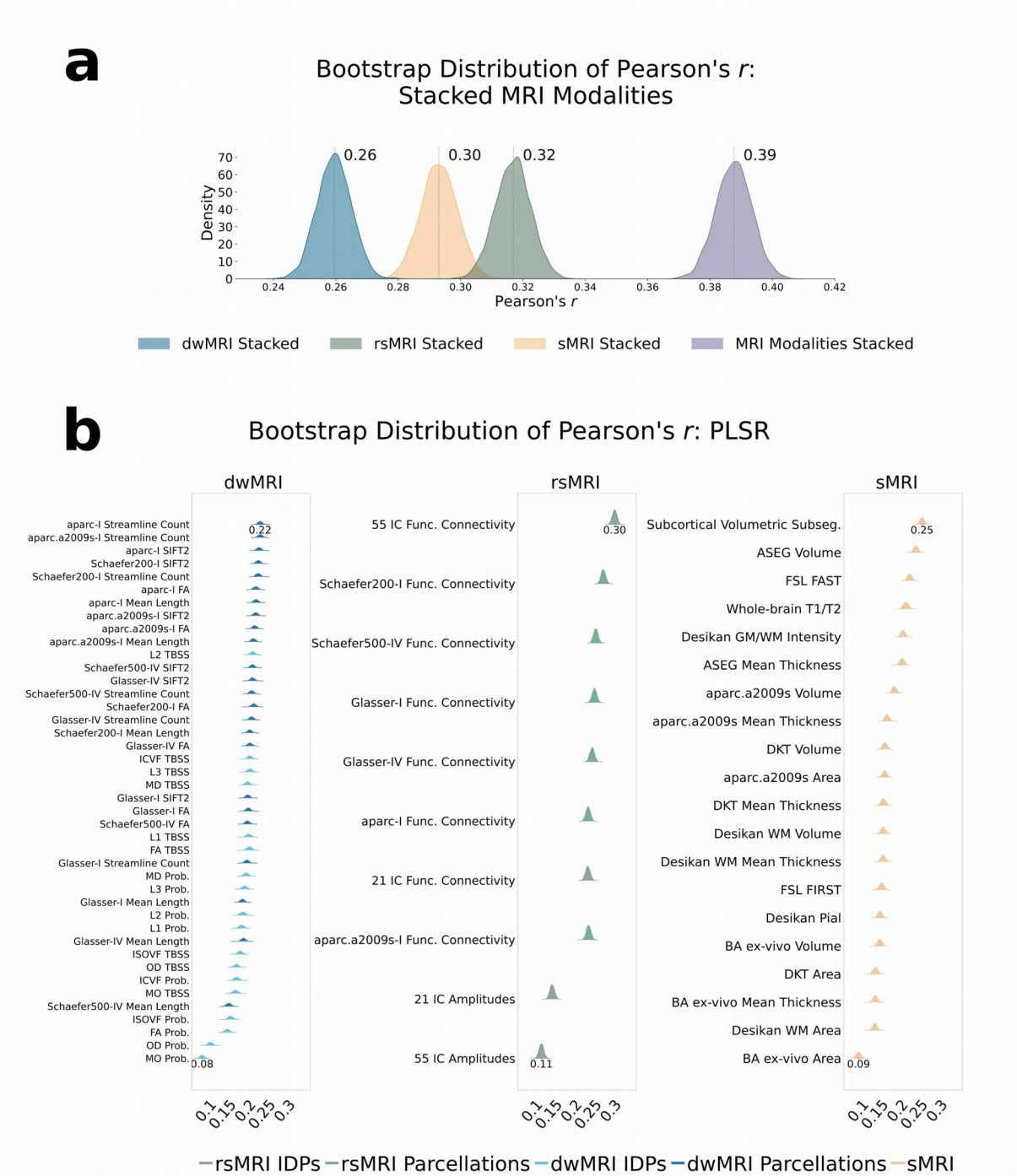

17

Figure 3. Performance of machine learning models in predicting the *g*-factor based on neuroimaging phenotypes and stacked MRI modalities. a Bootstrap distribution of Pearson *r* between the *g*-factor derived from ESEM and the *g*-factor predicted from stacked dwMRI, rsMRI, sMRI, and all MRI modalities stacked. Values at the top of each plot mark median Pearson *r*. **b** Bootstrap distribution of Pearson *r* for the *g*-factor derived from ESEM and *g*-factor predicted from each neuroimaging phenotype. Values at the top and bottom of the plots mark the median Pearson *r*.

Commonality Analysis

Different neuroimaging phenotypes captured the relationship between cognition and mental health at varying degrees, as indicated by a percentage ratio between the common effect of mental health-*g* and neuroimaging-*g* and the total effect of mental health-*g*. Neuroimaging phenotypes from dwMRI, rsMRI, and sMRI accounted for 2.1%–19.3%, 4%–25.8%, and 4.8%–21.8% of the cognition-mental health relationship, respectively (Fig. 4b and Supplementary Tables 18 and 19). Among dwMRI neuroimaging phenotypes, the number of streamlines connecting grey matter regions from Destrieux (aparc.a2009s) cortical + MSA-I subcortical parcellations shared the highest proportion of variance with mental health-*g* (19.3%). For rsMRI, the largest proportion of the common effect of mental health-*g* was shared with RSFC between 55 ICs (25.8%). For sMRI, subcortical volumetric subsegmentaion contributed most to the link between cognition and mental health (21.8%). The correlation between the performance of each neuroimaging phenotype in predicting cognition and the proportion of the relationship between cognition and mental health captured by the phenotype was $r = 0.97$ (Fig. 4a).

18

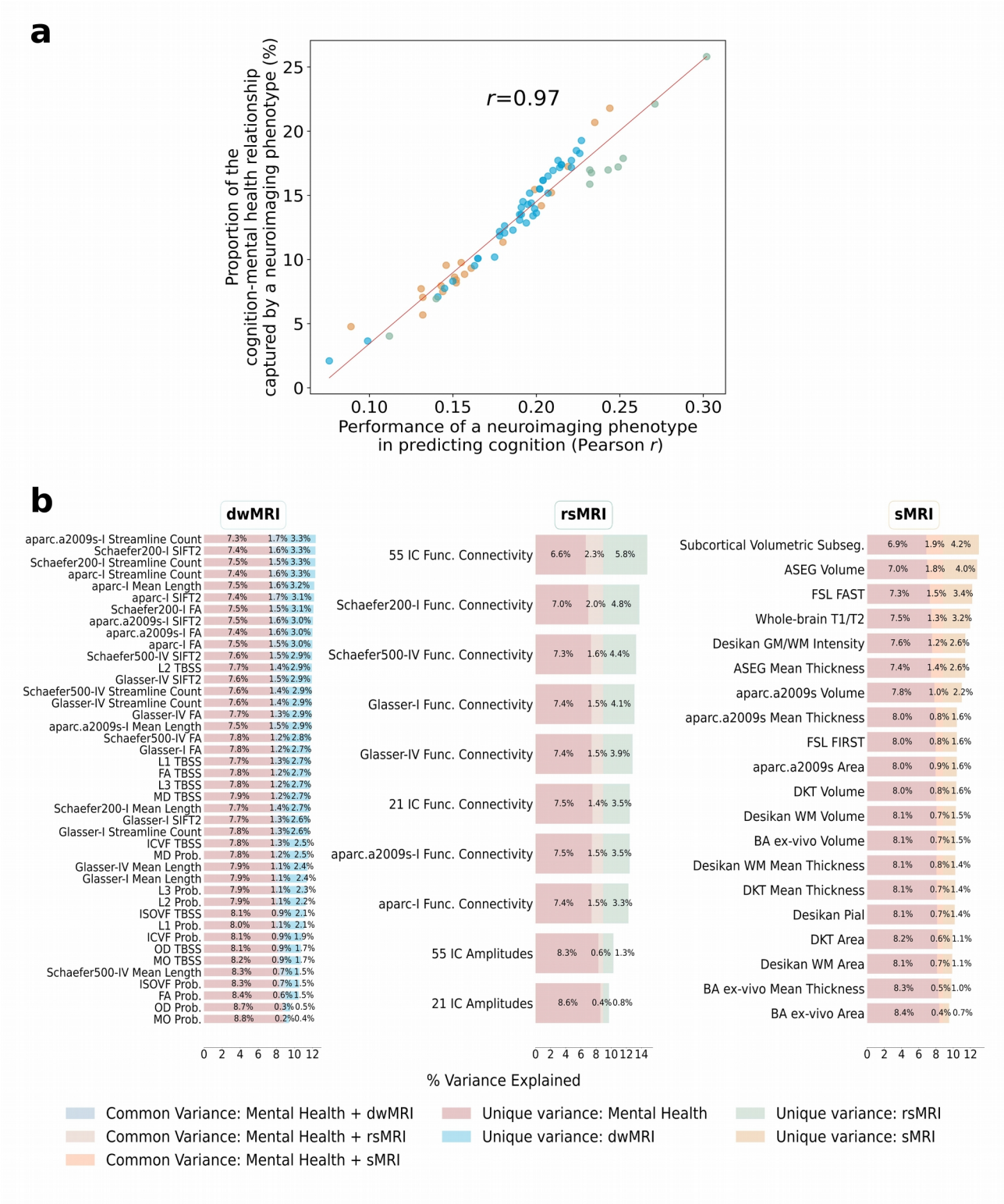

Figure 4. The contribution of neuroimaging phenotypes to the relationship between cognition and mental health: Results of commonality analyses. a Scatterplot of the relationship between the PLSR performance of individual neuroimaging phenotypes and the proportion of cognition-mental health relationship they capture. **b** Stacked barplot diagrams of the results of commonality analyses for each neuroimaging phenotype. *Unique variance* proportion (%) of

variance in the *g*-factor explained uniquely by mental health and neuroimaging phenotypes, *Common variance* proportion (%) of variance in the *g*-factor shared between mental health and neuroimaging phenotypes. *aparc.a2009s* Destrieux cortical atlas, *Schaefer7n200p* Schaefer Atlas for 7 networks and 200 parcels, *Schaefer7n500p* Schaefer Atlas for 7 networks and 500 parcels, *I* Melbourne Subcortical Atlas I, *IV* Melbourne Subcortical Atlas IV, *SIFT2* Spherical-Deconvolution Informed Filtering of Tractograms 2, *FA* fractional anisotropy, *MD* mean diffusivity, *MO* diffusion tensor mode, *L1, L2, L3* eigenvalues of the diffusion tensor, *OD* orientation dispersion index, *ICVF* intracellular volume fraction, *ISOVF* isotropic volume fraction, *TBSS* Tract-Based Spatial Statistics, *Func. Connectivity* functional connectivity, *Subseg*. subsegmentation, *ASEG* Freesurfer automated subcortical volumetric segmentation, *FSL FAST* FSL FMRIB's Automated Segmentation Tool, *WM* white matter, *GM* grey matter, *FSL FIRST* FMRIB's Integrated Registration and Segmentation Tool, *DKT* Desikan-Killiany-Tourville, *BA* FreeSurfer *ex-vivo* Brodmann Area Maps.

When we stacked neuroimaging phenotypes within dwMRI, rsMRI, and sMRI, we captured 25.5%, 29.8%, and 31.6% of the predictive relationship between cognition and mental health, respectively. By stacking all 72 neuroimaging phenotypes across three MRI modalities, we enhanced the explanation to 48% (Fig. 5 e–h and Supplementary Table 20). Age and sex contributed considerably to the relationship between cognition, mental health, and MRI. In particular, the common effects shared by the three predictors were 2%, 1.3%, 2.5%, and 2.8% for models incorporating dwMRI, rsMRI, sMRI, and all MRI modalities stacked, respectively (Fig. 5 i–l and Supplementary Table 21).

20

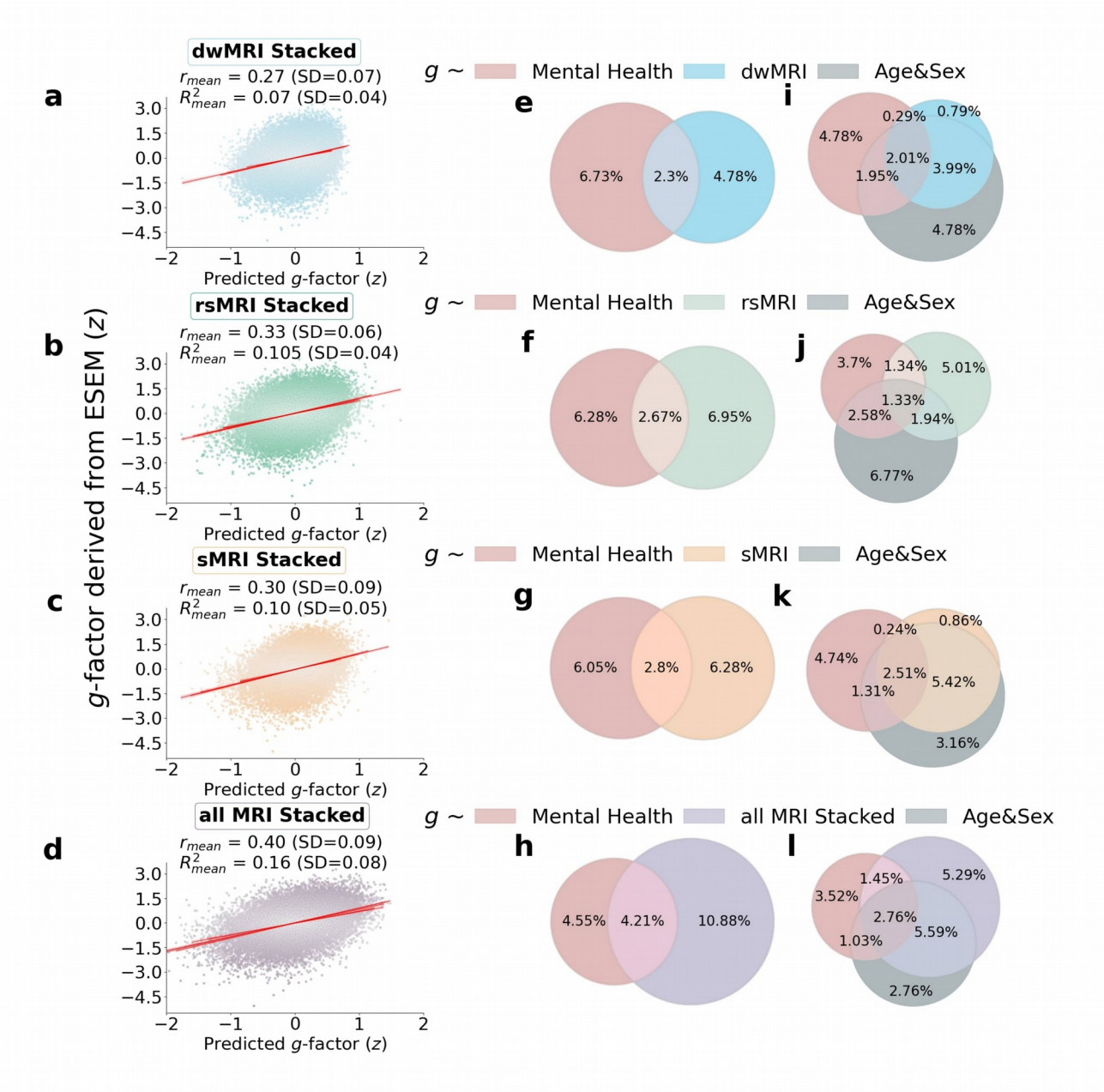

Figure 5. The contribution of neuroimaging phenotypes stacked within each and across all MRI modalities to the relationship between cognition and mental health: Results of predictive modeling and commonality analyses. a-d Distributions of the *g*-factor derived from cognitive tests via ESEM and predicted from stacked dwMRI **(a)**, rsMRI **(b)**, sMRI **(c)**, and all MRI modalities **(d)**. **e-l** Venn diagrams of the results of commonality analyses. **e-h** The proportion (%) of variance in the *g*-factor explained uniquely by mental health and neuroimaging phenotypes: dwMRI **(e)**, rsMRI **(f)**, sMRI **(g)**, and all MRI modalities stacked **(h)**, as well as the common effects between mental health and neuroimaging phenotypes. **i-l** The proportion (%) of variance in the *g*-factor explained uniquely by mental health, neuroimaging phenotypes stacked within dwMRI **(i),** rsMRI **(j)**, sMRI **(k)**, and all MRI modalities **(l)**, and age and sex, as well as the common effects among all explanatory variables.

Discussion

Our study is the first to quantify the contribution of the neural indicators of cognition, as reflected by the *g*-factor, to its relationship with mental health in the largest population-level cohort. We show that the performance of each neural indicator in predicting cognition *per se* is strongly related to its ability to explain the link between cognition and mental health. In other words, the "robustness" of the neural indicator of cognition is associated with its capacity to capture the covariation between cognition and mental health. This means that the neural indicators that capture more of the individual differences in cognition also capture more of the cognition-mental health covariation. We further demonstrate that information from 72 neuroimaging phenotypes from three MRI modalities accounts for almost half of the variance in the relationship between cognition and mental health. Aspects of the brain that underpin this relationship are best reflected in neuroimaging phenotypes derived from rsMRI followed by sMRI and dwMRI. For rsMRI, RSFC between 55 large-scale networks measured with tangent space parameterization was the best-performing neuroimaging phenotype. Among sMRI neuroimaging phenotypes, subcortical grey matter characteristics quantified with subcortical volumetric subsegmentation and FreeSurfer's ASEG shared the highest proportion of the variance that mental health captures. For dwMRI, microstructural properties of the brain's white matter that underlie the link between cognition and mental health were best reflected in the number of streamlines connecting grey matter regions from Destrieux cortical + MSA I subcortical parcellations. Integrating information from neuroimaging phenotypes within and across MRI modalities enhanced both the prediction of cognition and the explanation of the relationship between cognition and mental health. We discuss the results in the context of current knowledge in the field, as follows.

The cognition and mental health relationship

We were able to predict cognition from 133 mental health indices, demonstrating a medium-sized relationship that aligns with the literature [60]. We also validated the quantification of cognition via the *g*-factor [31] showing that the *g*-factor captures almost half (39%) of the variance across twelve

22

cognitive performance scores, in agreement with previous studies [61–66]. Mental health was predictive of the *g*-factor at $R^2 = 0.10$ and $r = 0.31$.

The directions of factor loadings for mental health in the PLSR model allowed us to quantify the contribution of individual mental health indices to cognition. Overall, the scores for mental distress, alcohol and cannabis use, and self-harm behaviours relate positively, and the scores for anxiety, neurological and mental health diagnoses, unusual or psychotic experiences, happiness and subjective well-being, and negative traumatic events relate negatively to cognition, as indicated by factor loadings. We elaborate on these findings in Supplementary Materials (S12).

How well does MRI capture the predictive relationship between cognition and mental health?

Consistent with previous studies, we show that MRI data predict individual differences in cognition with a medium-size performance ($r \approx 0.4$) [15–17, 28, 61, 67, 68]. This provides us confidence in using MRI to derive quantitative neuromarkers of cognition. We further demonstrate that neural indicators of cognition derived from all neuroimaging phenotypes capture almost half (48%) of the variance in the cognition-mental health relationship. Neural indicators of cognition derived from rsMRI and sMRI neuroimaging phenotypes account for approximately a third of this link (29.8% and 31.6%, respectively). Yet, although rsMRI at a neuroimaging phenotype level and sMRI at a modality level are the most reflective of this relationship, combining all neuroimaging phenotypes from three MRI modalities allowed us to explain the highest proportion of the variance in cognition that mental health captures.

Among dwMRI-derived neuroimaging phenotypes, streamline count from grey matter parcellations results in a neural indicator that best reflects microstructural resources associated with cognition, as indicated by predictive modeling, and more importantly, shares the highest proportion of the variance with mental health-*g*, as indicated by commonality analysis. One of the mechanisms that can be reflected in the link between streamline count and individual variations in cognition is strengthening local connections within a hemisphere and enhancing local (i.e., the connectivity between neighbouring regions) and nodal efficiency (i.e., how well a given brain region is

23

connected to other regions) [69]. The limited utility of diffusion metrics obtained from probabilistic tractography in serving as a quantitative neuromarker of cognition and capturing its predictive relationship with mental health may be due to their higher specificity to neuronal damage or myelin loss rather than cognitive processing. While these indices can capture abnormal white matter microstructure in clinical populations such as Alzheimer's disease, schizophrenia, or attention deficit hyperactivity disorder (ADHD) [70–72], the empirical evidence on their associations with cognitive performance is controversial [71, 73–77]. One potential explanation is that these metrics are not specific to the properties of individual white matter axons or bundles, and instead represent a composite of multiple diffusion components averaged within a voxel and across major fibre pathways [78, 79].

We extend findings on the superior performance of rsMRI in predicting cognition, which aligns with the literature [15, 28], by showing that it also explains almost a third of the variance in cognition that mental health captures. At the neuroimaging phenotype level, this contribution is mostly driven by RSFC between 55 networks from ICA quantified with tangent space parameterization. ICA is a data-driven technique that does not rely on predefined anatomical boundaries. It captures intrinsic large-scale functional networks accounting for individual variability in RSFC. Thus, by providing more "personalized" connectivity representations, ICA-derived networks may be more robust neuronal indicators of cognitive performance than node-to-node estimates [80, 81]. Furthermore, using tangent space parametrization to quantify RSFC not only improves the predictive performance of rsMRI for cognition as shown previously [55, 82–85] but also allows us to capture more variance that cognition shares with mental health. Although tangent parametrization matrices do not reflect individual functional brain connections and cannot be interpreted directly, the linearization and projection to Euclidean space make functional connectivity estimates more suitable for statistical analysis and machine learning [54]. Resting-state fluctuation amplitudes from rsMRI which are the least predictive of cognition and explain the smallest proportion of the variance in cognition that mental health captures are believed to reflect

24

cardiovascular and cerebrovascular factors distinct from neural effects [86]. Research indicates that network amplitudes are significantly influenced by age, cardiovascular and lung function, and other physical measures, and are therefore subject to high interindividual variability. Consequently, interindividual variability in vascular health and aging dynamics may confront the capacity of network amplitudes to serve as a robust neuromarker of cognition [52].

Integrating information about brain anatomy by stacking sMRI neuroimaging phenotypes allowed us to explain a third of the link between cognition and mental health. Among all sMRI neuroimaging phenotypes, those that quantified the morphology of subcortical structures explain the highest portion of the variance in cognition captured by mental health. This may mean that subcortical structures, at least in older adults, contribute more to the brain-cognition relationship than variations in cortical grey and white matter which are more distributed and possess higher compensatory capacity. This aligns with the Scaffolding Theory which proposes stronger compensatory engagement of subcortical structures in cognitive processing in older adults [87–89].

The study has several limitations. First, the UK Biobank MRI data include only one task for task functional MRI (tfMRI), the Hariri hammer task [90], which is not designed to be cognitively demanding. Compared to other MRI modalities, tfMRI from certain tasks, such as the *n*-back working memory task [91], has been shown to provide the most robust neuromarker of cognition [17]. Thus, by not including cognitively demanding tfMRI tasks in predictive models we may have missed condition-specific variance that may account for a substantial portion of the variance specific to particular cognitive domains. Second, for generalizability purposes, we did not stratify the cohort nor exclude individuals with neurological, cardiovascular, or any other clinically established disorders, assuming that, in older adults, these effects can be tightly intertwined with neuronal mechanisms that sustain cognitive processing. Finally, the UK Biobank's mental health questionnaire and cognitive test battery may miss important information as they cover a limited and specific set of neuropsychiatric conditions and cognitive domains, respectively. For example, the mental health questionnaire does not include questions evaluating autism or ADHD symptoms. The

25

UK Biobank's cognitive test battery was designed specifically for the study and is different from commonly used cognitive test batteries such as the NIH Toolbox for Assessment of Neurological and Behavioral Function [92] used in the Human Connectome Project [93] and Adolescent Brain Cognitive Development Study [94] or Wechsler Adult Intelligence Scale [95] used in the Dunedin Study [96], which hinders the cross-study comparison of the cognitive performance score.

Overall, our findings suggest that RSFC is a more fine-tuned system that exhibits a degree of flexibility and variability that is not entirely constrained by anatomical pathways as cortical regions can use alternative or parallel pathways to strengthen or weaken functional connections underlying cognitive processing [97]. Although RSFC is believed to reflect anatomical connectivity [97, 98], alterations in structural connectivity do not always compromise RSFC [98]. From this point, a pattern of RSFC maintained for an extended period may eventually cause concurrent alterations in cognition and mental health, especially if it involves brain areas that have overlapping effects on both. Still, the physical integrity and morphology of the structures providing a "physical" relay for functionally connected brain areas to communicate play a pivotal role in the brain-behaviour relationship. Although more rigid and less flexible in an adult brain, they determine the amount of neural resources available for cognitive processing. Nevertheless, none of the neuroimaging phenotypes or MRI modalities alone is sufficient to provide a complete picture of the complex relationship between cognition and mental health, and combining all sources of information about brain structure and function reflected in three MRI modalities allows us to derive robust quantitative neuromarkers of cognition and boost explanation of neural correlates that underlie this link.

In line with the National Institute of Mental Health's Research Domain Criteria (RDoC) framework, we shed light on the relationship between cognition and mental health as one of the six transdiagnostic spectrums of neuropsychiatric symptoms at one of the seven units of analysis, i.e., the neural level [99]. This may serve as a methodological "bridge" linking other units of analysis such as genes and behaviour. By elucidating the role of different neuroimaging phenotypes as neural correlates of cognition that overlap with mental health, we provide potential targets for

26

behavioural and physiological interventions that may affect cognition. Our findings lay the foundation for further investigation of the specific neural mechanisms captured by dwMRI, rsMRI, and sMRI that underlie this relationship.

Data availability

The data used in this study are subject to the restrictions. Requests for access should be directed to UK Biobank (https://www.ukbiobank.ac.uk/).

Code availability

The codes for analyzing the data are available at https://github.com/HAM-lab-Otago-University/UKBiobank/.

Acknowledgments

This research has been conducted using the UK Biobank Resource under Applications Number 70132 and 633846. We are thankful to Professor Bruce Russell for his assistance with access to the UK Biobank dataset. N.P. and J.D. were supported by New Zealand Health Research Council Funding (grant number 21/618 and 24/838) and by Neurological Foundation of New Zealand (grant number 2350 PRG). I.B. was supported by the University of Otago.

Conflict of Interest

The authors declare that they have no conflict of interest to disclose.

27

References

1. Iosifescu DV. The relation between mood, cognition and psychosocial functioning in psychiatric disorders. Eur Neuropsychopharmacol J Eur Coll Neuropsychopharmacol. 2012;22 Suppl 3:S499–504.
2. Nyberg J, Henriksson M, Wall A, Vestberg T, Westerlund M, Walser M, et al. Anxiety severity and cognitive function in primary care patients with anxiety disorder: a cross-sectional study. BMC Psychiatry. 2021;21:617.
3. Gulpers BJA, Verhey FRJ, Eussen SJPM, Schram MT, de Galan BE, van Boxtel MPJ, et al. Anxiety and cognitive functioning in the Maastricht study: A cross-sectional population study. J Affect Disord. 2022;319:570–579.
4. Richardson L, Adams S. Cognitive deficits in patients with depression. J Nurse Pract. 2018;14:437–443.e3.
5. Wen M, Dong Z, Zhang L, Li B, Zhang Y, Li K. Depression and cognitive impairment: current understanding of its neurobiology and diagnosis. Neuropsychiatr Dis Treat. 2022;18:2783–2794.
6. Kriesche D, Woll CFJ, Tschentscher N, Engel RR, Karch S. Neurocognitive deficits in depression: a systematic review of cognitive impairment in the acute and remitted state. Eur Arch Psychiatry Clin Neurosci. 2023;273:1105–1128.
7. Fusar-Poli P, Deste G, Smieskova R, Barlati S, Yung AR, Howes O, et al. Cognitive functioning in prodromal psychosis: a meta-analysis. Arch Gen Psychiatry. 2012;69:562–571.
8. Mesholam-Gately RI, Giuliano AJ, Goff KP, Faraone SV, Seidman LJ. Neurocognition in first-episode schizophrenia: a meta-analytic review. Neuropsychology. 2009;23:315–336.
9. Guo JY, Ragland JD, Carter CS. Memory and cognition in schizophrenia. Mol Psychiatry. 2019;24:633–642.
10. Lindgren M, Birling H, Kieseppä T, Tuulio-Henriksson A. Is cognitive performance

28

associated with anxiety and depression in first-episode psychosis? J Affect Disord. 2020;263:221–227.

11. Chavez-Baldini U, Nieman DH, Keestra A, Lok A, Mocking RJT, de Koning P, et al. The relationship between cognitive functioning and psychopathology in patients with psychiatric disorders: a transdiagnostic network analysis. Psychol Med;53:476–485.

12. Semkovska M, Quinlivan L, O'Grady T, Johnson R, Collins A, O'Connor J, et al. Cognitive function following a major depressive episode: a systematic review and meta-analysis. Lancet Psychiatry. 2019;6:851–861.

13. Harvey PD, Bowie CR. Cognition in severe mental illness: Schizophrenia, bipolar disorder, and depression. In: Husain M, Schott JM (eds). Oxford Textbook of Cognitive Neurology and Dementia. Oxford University Press: Oxford, 2016.

14. Grotzinger AD, Cheung AK, Patterson MW, Harden KP, Tucker-Drob EM. Genetic and environmental links between: General factors of psychopathology and cognitive ability in early childhood. Clin Psychol Sci J Assoc Psychol Sci. 2019;7:430–444.

15. Pat N, Wang Y, Anney R, Riglin L, Thapar A, Stringaris A. Longitudinally stable, brain-based predictive models mediate the relationships between childhood cognition and socio-demographic, psychological and genetic factors. Hum Brain Mapp. 2022;43:5520–5542.

16. Krämer C, Stumme J, da Costa Campos L, Dellani P, Rubbert C, Caspers J, et al. Prediction of cognitive performance differences in older age from multimodal neuroimaging data. GeroScience. 2024;46:283–308.

17. Tetereva A, Li J, Deng JD, Stringaris A, Pat N. Capturing brain cognition relationship: Integrating task-based fMRI across tasks markedly boosts prediction and test-retest reliability. NeuroImage. 2022;263:119588.

18. Marek S, Tervo-Clemmens B, Calabro FJ, Montez DF, Kay BP, Hatoum AS, et al. Reproducible brain-wide association studies require thousands of individuals. Nature.

2022;603:654–660.

19. Zhi D, Jiang R, Pearlson G, Fu Z, Qi S, Yan W, et al. Triple interactions between the environment, brain, and behavior in children: An ABCD study. Biol Psychiatry. 2024;95:828–838.

20. Wang Y, Anney R, Pat N. Empirically validate cognitive abilities as an RDoC transdiagnostic domain for mental health across neural and genetic units of analysis. medRxiv, 2024-02.

21. Alexander AL, Lee JE, Lazar M, Field AS. Diffusion tensor imaging of the brain. Neurother J Am Soc Exp Neurother. 2007;4:316–329.

22. Soares JM, Marques P, Alves V, Sousa N. A hitchhiker's guide to diffusion tensor imaging. Front Neurosci. 2013;7:31.

23. Zhang H, Schneider T, Wheeler-Kingshott CA, Alexander DC. NODDI: practical in vivo neurite orientation dispersion and density imaging of the human brain. NeuroImage. 2012;61:1000–1016.

24. Basser PJ, Mattiello J, LeBihan D. MR diffusion tensor spectroscopy and imaging. Biophys J. 1994;66:259–267.

25. Lee MH, Smyser CD, Shimony JS. Resting-State fMRI: A Review of methods and clinical applications. AJNR Am J Neuroradiol. 2013;34:1866–1872.

26. Wattjes MP. Structural MRI. Int Psychogeriatr. 2011;23 Suppl 2:S13–24.

27. Symms M, Jäger HR, Schmierer K, Yousry TA. A review of structural magnetic resonance neuroimaging. J Neurol Neurosurg Psychiatry. 2004;75:1235–1244.

28. Dhamala E, Jamison KW, Jaywant A, Dennis S, Kuceyeski A. Distinct functional and structural connections predict crystallised and fluid cognition in healthy adults. Hum Brain Mapp. 2021;42:3102–3118.

29. Caunca MR, Wang L, Cheung YK, Alperin N, Lee SH, Elkind MSV, et al. Machine learning-based estimation of cognitive performance using regional brain MRI markers:

the Northern Manhattan Study. Brain Imaging Behav. 2021;15:1270–1278.

30. Rasero J, Sentis AI, Yeh F-C, Verstynen T. Integrating across neuroimaging modalities boosts prediction accuracy of cognitive ability. PLOS Comput Biol. 2021;17:e1008347.

31. Jensen AR. The g factor: psychometrics and biology. Novartis Found Symp. 2000;233:37–47.

32. Panizzon MS, Vuoksimaa E, Spoon KM, Jacobson KC, Lyons MJ, Franz CE, et al. Genetic and environmental influences of general cognitive ability: Is g a valid latent construct? Intelligence. 2014;43:65–76.

33. Nimon K, Lewis M, Kane R, Haynes RM. An R package to compute commonality coefficients in the multiple regression case: An introduction to the package and a practical example. Behav Res Methods. 2008;40:457–466.

34. Fawns-Ritchie C, Deary IJ. Reliability and validity of the UK Biobank cognitive tests. PLoS ONE. 2020;15:e0231627.

35. Davis KAS, Coleman JRI, Adams M, Allen N, Breen G, Cullen B, et al. Mental health in UK Biobank – development, implementation and results from an online questionnaire completed by 157 366 participants: a reanalysis. BJPsych Open. 2020;6:e18.

36. Dutt RK, Hannon K, Easley TO, Griffis JC, Zhang W, Bijsterbosch JD. Mental health in the UK Biobank: A roadmap to self-report measures and neuroimaging correlates. Hum Brain Mapp. 2022;43:816–832.

37. Miller KL, Alfaro-Almagro F, Bangerter NK, Thomas DL, Yacoub E, Xu J, et al. Multimodal population brain imaging in the UK Biobank prospective epidemiological study. Nat Neurosci. 2016;19:1523–1536.

38. Alfaro-Almagro F, Jenkinson M, Bangerter NK, Andersson JLR, Griffanti L, Douaud G, et al. Image processing and Quality Control for the first 10,000 brain imaging datasets from UK Biobank. Neuroimage. 2018;166:400–424.

39. Mansour L. S, Di Biase MA, Smith RE, Zalesky A, Seguin C. Connectomes for 40,000

UK Biobank participants: A multi-modal, multi-scale brain network resource. NeuroImage. 2023;283:120407.

40. Desikan RS, Ségonne F, Fischl B, Quinn BT, Dickerson BC, Blacker D, et al. An automated labeling system for subdividing the human cerebral cortex on MRI scans into gyral based regions of interest. NeuroImage. 2006;31:968–980.

41. Tian Y, Margulies DS, Breakspear M, Zalesky A. Topographic organization of the human subcortex unveiled with functional connectivity gradients. Nat Neurosci. 2020;23:1421–1432.

42. Destrieux C, Fischl B, Dale A, Halgren E. Automatic parcellation of human cortical gyri and sulci using standard anatomical nomenclature. NeuroImage. 2010;53:1–15.

43. Glasser MF, Coalson TS, Robinson EC, Hacker CD, Harwell J, Yacoub E, et al. A multi-modal parcellation of human cerebral cortex. Nature. 2016;536:171–178.

44. Schaefer A, Kong R, Gordon EM, Laumann TO, Zuo X-N, Holmes AJ, et al. Local-global parcellation of the human cerebral cortex from intrinsic functional connectivity MRI. Cereb Cortex. 2018;28:3095–3114.

45. Thomas Yeo BT, Krienen FM, Sepulcre J, Sabuncu MR, Lashkari D, Hollinshead M, et al. The organization of the human cerebral cortex estimated by intrinsic functional connectivity. J Neurophysiol. 2011;106:1125–1165.

46. Smith SM, Jenkinson M, Johansen-Berg H, Rueckert D, Nichols TE, Mackay CE, et al. Tract-based spatial statistics: voxelwise analysis of multi-subject diffusion data. NeuroImage. 2006;31:1487–1505.

47. Behrens TEJ, Woolrich MW, Jenkinson M, Johansen-Berg H, Nunes RG, Clare S, et al. Characterization and propagation of uncertainty in diffusion-weighted MR imaging. Magn Reson Med. 2003;50:1077–1088.

48. Behrens TEJ, Berg HJ, Jbabdi S, Rushworth MFS, Woolrich MW. Probabilistic diffusion tractography with multiple fibre orientations: What can we gain? NeuroImage.

 32

2007;34:144–155.

49. Jbabdi S, Sotiropoulos SN, Savio AM, Graña M, Behrens TEJ. Model-based analysis of multishell diffusion MR data for tractography: how to get over fitting problems. Magn Reson Med. 2012;68:1846–1855.

50. Glasser MF, Sotiropoulos SN, Wilson JA, Coalson TS, Fischl B, Andersson JL, et al. The minimal preprocessing pipelines for the Human Connectome Project. NeuroImage. 2013;80:105–124.

51. Andersson JLR, Sotiropoulos SN. An integrated approach to correction for off-resonance effects and subject movement in diffusion MR imaging. NeuroImage. 2016;125:1063–1078.

52. Lee S, Bijsterbosch JD, Almagro FA, Elliott L, McCarthy P, Taschler B, et al. Amplitudes of resting-state functional networks – investigation into their correlates and biophysical properties. NeuroImage. 2023;265:119779.

53. Abbas K, Liu M, Wang M, Duong-Tran D, Tipnis U, Amico E, et al. Tangent functional connectomes uncover more unique phenotypic traits. iScience. 2023;26:107624.

54. Pervaiz U, Vidaurre D, Woolrich MW, Smith SM. Optimising network modelling methods for fMRI. NeuroImage. 2020;211:116604.

55. Ng B, Dressler M, Varoquaux G, Poline JB, Greicius M, Thirion B. Transport on Riemannian Manifold for Functional Connectivity-Based Classification. In: Golland P, Hata N, Barillot C, Hornegger J, Howe R, editors. Med. Image Comput. Comput.-Assist. Interv. – MICCAI 2014, Cham: Springer International Publishing, 2014, pp 405–412.

56. Zhang Y, Brady M, Smith S. Segmentation of brain MR images through a hidden Markov random field model and the expectation-maximization algorithm. IEEE Trans Med Imaging. 2001;20:45–57.

57. Patenaude B, Smith SM, Kennedy DN, Jenkinson M. A Bayesian model of shape and appearance for subcortical brain segmentation. NeuroImage. 2011;56:907–922.

33

58. Iglesias JE, Augustinack JC, Nguyen K, Player CM, Player A, Wright M, et al. A computational atlas of the hippocampal formation using ex vivo, ultra-high resolution MRI: Application to adaptive segmentation of in vivo MRI. NeuroImage. 2015;115:117–137.

59. Alfaro-Almagro F, McCarthy P, Afyouni S, Andersson JLR, Bastiani M, Miller KL, et al. Confound modelling in UK Biobank brain imaging. NeuroImage. 2021;224:117002.

60. Abramovitch A, Short T, Schweiger A. The C Factor: Cognitive dysfunction as a transdiagnostic dimension in psychopathology. Clin Psychol Rev. 2021;86:102007.

61. Dubois J, Galdi P, Paul LK, Adolphs R. A distributed brain network predicts general intelligence from resting-state human neuroimaging data. Philos Trans R Soc B Biol Sci. 2018;373:20170284.

62. Gignac GE, Bates TC. Brain volume and intelligence: The moderating role of intelligence measurement quality. Intelligence. 2017;64:18–29.

63. Gignac GE, Szodorai ET. Defining intelligence: Bridging the gap between human and artificial perspectives. Intelligence. 2024;104:101832.

64. Canivez GL, Watkins MW. Investigation of the factor structure of the Wechsler Adult Intelligence Scale—Fourth Edition (WAIS–IV): Exploratory and higher order factor analyses. Psychol Assess. 2010;22:827–836.

65. Dombrowski SC, McGill RJ, Canivez GL. Hierarchical exploratory factor analyses of the Woodcock-Johnson IV Full Test Battery: Implications for CHC application in school psychology. Sch Psychol Q. 2018;33:235–250.

66. Galsworthy MJ, Paya-Cano JL, Liu L, Monleón S, Gregoryan G, Fernandes C, et al. Assessing reliability, heritability and general cognitive ability in a battery of cognitive tasks for laboratory mice. Behav Genet. 2005;35:675–692.

67. Sripada C, Rutherford S, Angstadt M, Thompson WK, Luciana M, Weigard A, et al. Prediction of neurocognition in youth from resting state fMRI. Mol Psychiatry.

34

2020;25:3413–3421.

68. He T, Kong R, Holmes AJ, Nguyen M, Sabuncu MR, Eickhoff SB, et al. Deep neural networks and kernel regression achieve comparable accuracies for functional connectivity prediction of behavior and demographics. NeuroImage. 2020;206:116276.

69. Neudorf J, Shen K, McIntosh AR. Reorganization of structural connectivity in the brain supports preservation of cognitive ability in healthy aging. Netw Neurosci. 2024:1–23.

70. Douaud G, Jbabdi S, Behrens TEJ, Menke RA, Gass A, Monsch AU, et al. DTI measures in crossing-fibre areas: Increased diffusion anisotropy reveals early white matter alteration in MCI and mild Alzheimer's disease. NeuroImage. 2011;55:880–890.

71. Bergamino M, Walsh RR, Stokes AM. Free-water diffusion tensor imaging improves the accuracy and sensitivity of white matter analysis in Alzheimer's disease. Sci Rep. 2021;11:6990.

72. Silk TJ, Vance A, Rinehart N, Bradshaw JL, Cunnington R. White-matter abnormalities in attention deficit hyperactivity disorder: a diffusion tensor imaging study. Hum Brain Mapp. 2009;30:2757–2765.

73. Bozzali M, Falini A, Franceschi M, Cercignani M, Zuffi M, Scotti G, et al. White matter damage in Alzheimer's disease assessed in vivo using diffusion tensor magnetic resonance imaging. J Neurol Neurosurg Psychiatry. 2002;72:742–746.

74. Shim G, Choi K-Y, Kim D, Suh S-I, Lee S, Jeong H-G, et al. Predicting neurocognitive function with hippocampal volumes and DTI metrics in patients with Alzheimer's dementia and mild cognitive impairment. Brain Behav. 2017;7:e00766.

75. Patil RB, Ramakrishnan S. Analysis of sub-anatomic diffusion tensor imaging indices in white matter regions of Alzheimer with MMSE score. Comput Methods Programs Biomed. 2014;117:13–19.

76. Stahl R, Dietrich O, Teipel SJ, Hampel H, Reiser MF, Schoenberg SO. White matter damage in Alzheimer disease and mild cognitive impairment: assessment with diffusion-

tensor MR imaging and parallel imaging techniques. Radiology. 2007;243:483–492.

77. Chen Y, Wang Y, Song Z, Fan Y, Gao T, Tang X. Abnormal white matter changes in Alzheimer's disease based on diffusion tensor imaging: A systematic review. Ageing Res Rev. 2023;87:101911.

78. Pierpaoli C, Jezzard P, Basser PJ, Barnett A, Di Chiro G. Diffusion tensor MR imaging of the human brain. Radiology. 1996;201:637–648.

79. O'Donnell LJ, Westin C-F. An introduction to diffusion tensor image analysis. Neurosurg Clin N Am. 2011;22:185–viii.

80. Marrelec G, Fransson P. Assessing the influence of different ROI selection strategies on functional connectivity analyses of fMRI data acquired during steady-state conditions. PLOS ONE. 2011;6:e14788.

81. Sohn WS, Yoo K, Lee Y-B, Seo SW, Na DL, Jeong Y. Influence of ROI selection on resting state functional connectivity: an individualized approach for resting state fMRI analysis. Front Neurosci. 2015;9:280.

82. Abbas K, Liu M, Wang M, Duong-Tran D, Tipnis U, Amico E, et al. Tangent functional connectomes uncover more unique phenotypic traits. iScience. 2023;26:107624.

83. Venkatesh M, Jaja J, Pessoa L. Comparing functional connectivity matrices: A geometry-aware approach applied to participant identification. NeuroImage. 2020;207:116398.

84. Simeon G, Piella G, Camara O, Pareto D. Riemannian geometry of functional connectivity matrices for multi-site attention-deficit/hyperactivity disorder data harmonization. Front Neuroinformatics. 2022;16:769274.

85. Dadi K, Rahim M, Abraham A, Chyzhyk D, Milham M, Thirion B, et al. Benchmarking functional connectome-based predictive models for resting-state fMRI. NeuroImage. 2019;192:115–134.

86. Tsvetanov KA, Henson RNA, Jones PS, Mutsaerts H, Fuhrmann D, Tyler LK, et al. The effects of age on resting-state BOLD signal variability is explained by cardiovascular and

cerebrovascular factors. Psychophysiology. 2021;58:e13714.

87. Reuter-Lorenz PA, Park DC. How Does it STAC Up? Revisiting the Scaffolding Theory of Aging and Cognition. Neuropsychol Rev. 2014;24:355–370.

88. Vieira BH, Rondinoni C, Garrido Salmon CE. Evidence of regional associations between age-related inter-individual differences in resting-state functional connectivity and cortical thinning revealed through a multi-level analysis. NeuroImage. 2020;211:116662.

89. Park DC, Reuter-Lorenz P. The Adaptive Brain: Aging and Neurocognitive Scaffolding. Annu Rev Psychol. 2009;60:173–196.

90. Hariri AR, Bookheimer SY, Mazziotta JC. Modulating emotional responses: effects of a neocortical network on the limbic system. Neuroreport. 2000;11:43–48.

91. Kirchner WK. Age differences in short-term retention of rapidly changing information. J Exp Psychol. 1958;55:352–358.

92. Gershon RC, Wagster MV, Hendrie HC, Fox NA, Cook KF, Nowinski CJ. NIH Toolbox for Assessment of Neurological and Behavioral Function. Neurology. 2013;80:S2.

93. Elam JS, Van Essen D. Human Connectome Project. In: Jaeger D, Jung R, editors. Encycl. Comput. Neurosci., New York, NY: Springer, 2022, pp 1647–1650.

94. Casey BJ, Cannonier T, Conley MI, Cohen AO, Barch DM, Heitzeg MM, et al. The Adolescent Brain Cognitive Development (ABCD) study: Imaging acquisition across 21 sites. Dev Cogn Neurosci. 2018;32:43–54.

95. Hartman DE. Wechsler Adult Intelligence Scale IV (WAIS IV): return of the gold standard. Appl Neuropsychol. 2009;16:85–87.

96. Poulton R, Moffitt TE, Silva PA. The Dunedin Multidisciplinary Health and Development Study: overview of the first 40 years, with an eye to the future. Soc Psychiatry Psychiatr Epidemiol. 2015;50:679.

97. Greicius MD, Supekar K, Menon V, Dougherty RF. Resting-state functional connectivity reflects structural connectivity in the default mode network. Cereb Cortex. 2009;19:72–

78.

98. O'Reilly JX, Croxson PL, Jbabdi S, Sallet J, Noonan MP, Mars RB, et al. Causal effect of disconnection lesions on interhemispheric functional connectivity in rhesus monkeys. Proc Natl Acad Sci USA. 2013;110:13982–13987.

99. Morris SE, Cuthbert BN. Research Domain Criteria: cognitive systems, neural circuits, and dimensions of behavior. Dialogues Clin Neurosci. 2012;14:29.

38

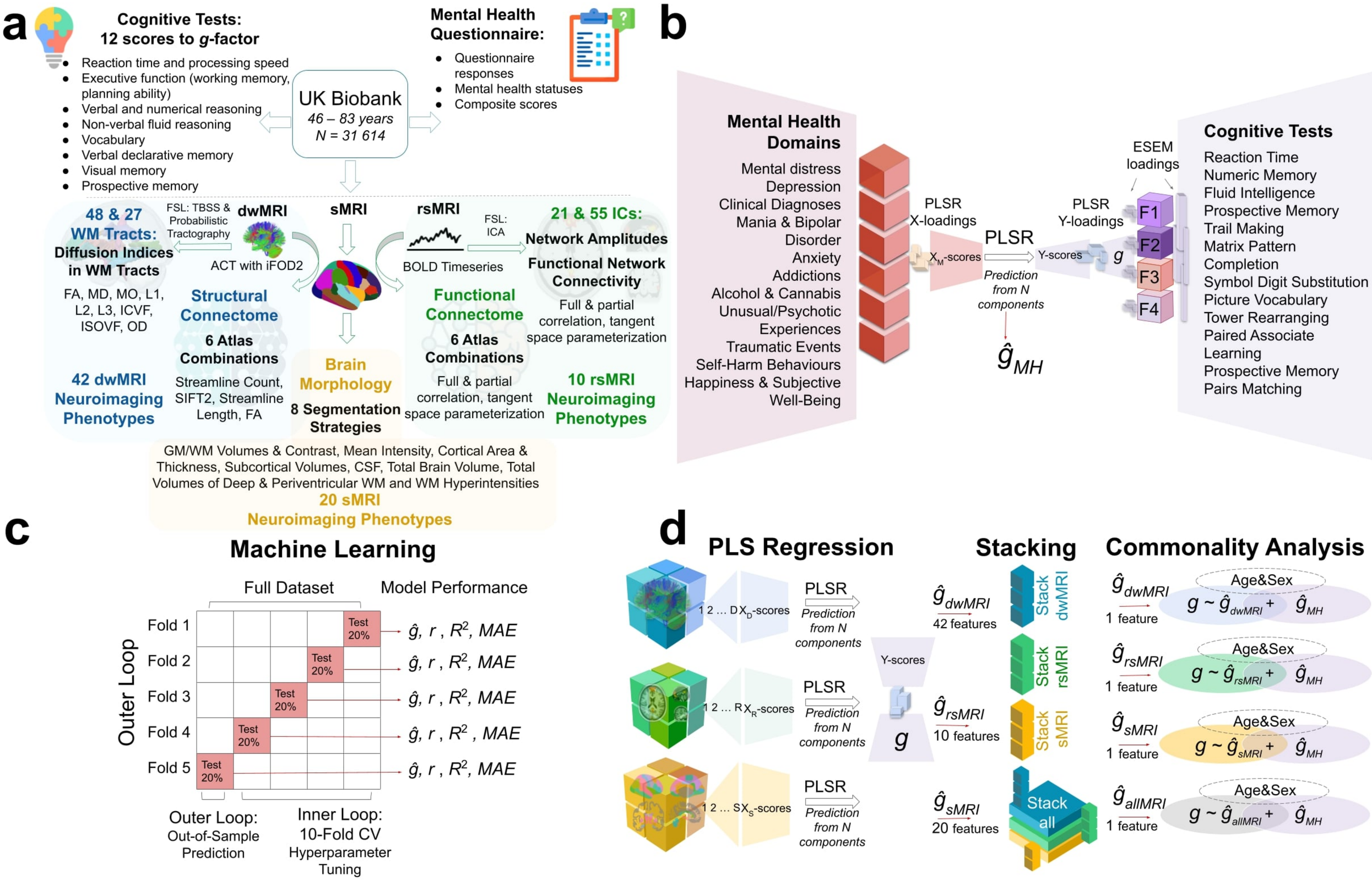
a
Cognitive Tests:
12 scores to g-factor
Reaction time and processing speed
Executive function (working memory, planning ability)
Verbal and numerical reasoning
Non-verbal fluid reasoning
Vocabulary
Verbal declarative memory
Visual memory
Prospective memory
UK Biobank
46 – 83 years
N = 31 614
Mental Health Questionnaire:
Questionnaire responses
Mental health statuses
Composite scores
48 & 27 WM Tracts:
Diffusion Indices in WM Tracts
FA, MD, MO, L1, L2, L3, ICVF, ISOVF, OD
FSL: TBSS & Probabilistic Tractography
dwMRI
ACT with iFOD2
sMRI
rsMRI
FSL: ICA
BOLD Timeseries
21 & 55 ICs:
Network Amplitudes
Functional Network Connectivity
Full & partial correlation, tangent space parameterization
Structural Connectome
6 Atlas Combinations
Streamline Count, SIFT2, Streamline Length, FA
Functional Connectome
6 Atlas Combinations
Full & partial correlation, tangent space parameterization
42 dwMRI Neuroimaging Phenotypes
Brain Morphology
8 Segmentation Strategies
10 rsMRI Neuroimaging Phenotypes
GM/WM Volumes & Contrast, Mean Intensity, Cortical Area & Thickness, Subcortical Volumes, CSF, Total Brain Volume, Total Volumes of Deep & Periventricular WM and WM Hyperintensities
20 sMRI
Neuroimaging Phenotypes
b
Mental Health Domains
Mental distress
Depression
Clinical Diagnoses
Mania & Bipolar Disorder
Anxiety
Addictions
Alcohol & Cannabis
Unusual/Psychotic Experiences
Traumatic Events
Self-Harm Behaviours
Happiness & Subjective Well-Being
PLSR X-loadings
X_M-scores
PLSR
Prediction from N components
$\hat{g}_{MH}$
Y-scores
PLSR Y-loadings
ESEM loadings
g
F1
F2
F3
F4
Cognitive Tests
Reaction Time
Numeric Memory
Fluid Intelligence
Prospective Memory
Trail Making
Matrix Pattern Completion
Symbol Digit Substitution
Picture Vocabulary
Tower Rearranging
Paired Associate Learning
Prospective Memory
Pairs Matching
c
Machine Learning
Full Dataset
Model Performance
Outer Loop
Fold 1
Fold 2
Fold 3
Fold 4
Fold 5
Test 20%
$\hat{g}$, r , R^2, MAE
Outer Loop: Out-of-Sample Prediction
Inner Loop: 10-Fold CV Hyperparameter Tuning
d
PLS Regression
1 2 … D X_D-scores
1 2 … R X_R-scores
1 2 … S X_S-scores
PLSR
Prediction from N components
Y-scores
g
Stacking
$\hat{g}_{dwMRI}$
42 features
$\hat{g}_{rsMRI}$
10 features
$\hat{g}_{sMRI}$
20 features
Stack dwMRI
Stack rsMRI
Stack sMRI
Stack all
Commonality Analysis
$\hat{g}_{dwMRI}$
1 feature
$\hat{g}_{rsMRI}$
$\hat{g}_{sMRI}$
$\hat{g}_{allMRI}$
Age&Sex
$g \sim \hat{g}_{dwMRI} + \hat{g}_{MH}$
$g \sim \hat{g}_{rsMRI} + \hat{g}_{MH}$
$g \sim \hat{g}_{sMRI} + \hat{g}_{MH}$
$g \sim \hat{g}_{allMRI} + \hat{g}_{MH}$

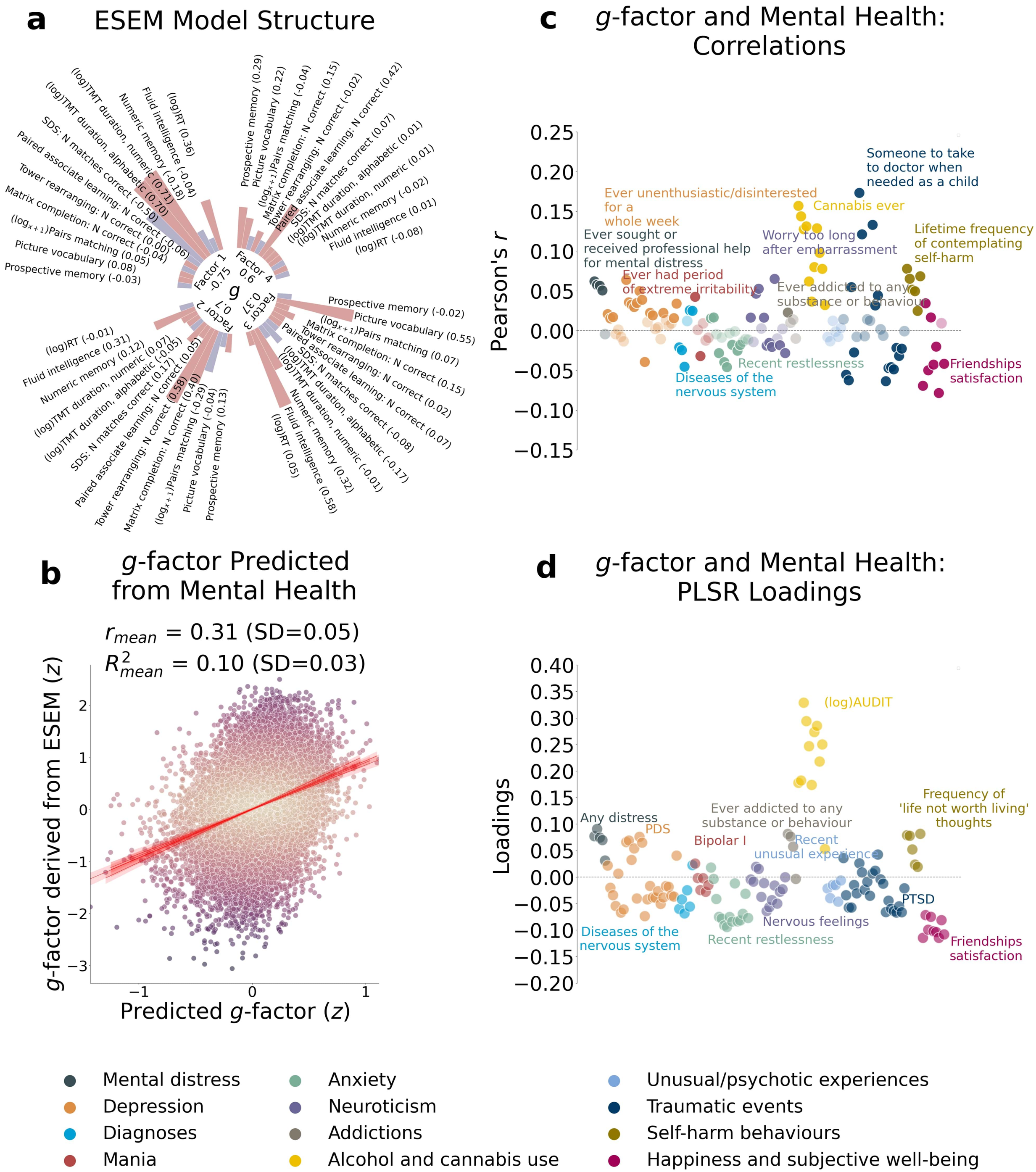
a
ESEM Model Structure
g
Factor 1 -0.75
Factor 2 0.7
Factor 3 0.37
Factor 4 0.6
(log)RT (0.36)
Fluid intelligence (-0.04)
Numeric memory (-0.18)
(log)TMT duration, numeric (0.71)
(log)TMT duration, alphabetic (0.70)
SDS: N matches correct (-0.50)
Paired associate learning: N correct (-0.06)
Tower rearranging: N correct (-0.00)
Matrix completion: N correct (-0.04)
(log$_{x+1}$)Pairs matching (0.05)
Picture vocabulary (0.08)
Prospective memory (-0.03)
Prospective memory (0.29)
Picture vocabulary (0.22)
(log$_{x+1}$)Pairs matching (-0.04)
Matrix completion: N correct (0.15)
Tower rearranging: N correct (-0.02)
Paired associate learning: N correct (0.42)
SDS: N matches correct (0.07)
(log)TMT duration, alphabetic (0.01)
(log)TMT duration, numeric (0.01)
Numeric memory (-0.02)
Fluid intelligence (0.01)
(log)RT (-0.08)
(log)RT (-0.01)
Fluid intelligence (0.31)
Numeric memory (0.12)
(log)TMT duration, numeric (0.07)
(log)TMT duration, alphabetic (-0.05)
SDS: N matches correct (0.17)
Paired associate learning: N correct (0.05)
Tower rearranging: N correct (0.58)
Matrix completion: N correct (0.40)
(log$_{x+1}$)Pairs matching (-0.29)
Picture vocabulary (-0.04)
Prospective memory (0.13)
Prospective memory (-0.02)
Picture vocabulary (0.55)
(log$_{x+1}$)Pairs matching (0.07)
Matrix completion: N correct (0.15)
Tower rearranging: N correct (0.02)
Paired associate learning: N correct (0.07)
SDS: N matches correct (-0.08)
(log)TMT duration, alphabetic (-0.17)
(log)TMT duration, numeric (-0.01)
Numeric memory (0.32)
Fluid intelligence (0.58)
(log)RT (0.05)
b
g-factor Predicted from Mental Health
r_{mean} = 0.31 (SD=0.05)
R^2_{mean} = 0.10 (SD=0.03)
g-factor derived from ESEM (z)
Predicted g-factor (z)
c
g-factor and Mental Health: Correlations
Pearson's r
Someone to take to doctor when needed as a child
Ever unenthusiastic/disinterested for a whole week
Cannabis ever
Ever sought or received professional help for mental distress
Worry too long after embarrassment
Lifetime frequency of contemplating self-harm
Ever had period of extreme irritability
Ever addicted to any substance or behaviour
Recent restlessness
Diseases of the nervous system
Friendships satisfaction
d
g-factor and Mental Health: PLSR Loadings
Loadings
(log)AUDIT
Frequency of 'life not worth living' thoughts
Ever addicted to any substance or behaviour
Any distress
PDS
Bipolar I
Recent unusual experience
PTSD
Nervous feelings
Diseases of the nervous system
Recent restlessness
Friendships satisfaction
Mental distress
Depression
Diagnoses
Mania
Anxiety
Neuroticism
Addictions
Alcohol and cannabis use
Unusual/psychotic experiences
Traumatic events
Self-harm behaviours
Happiness and subjective well-being

a

Bootstrap Distribution of Pearson's *r*: Stacked MRI Modalities

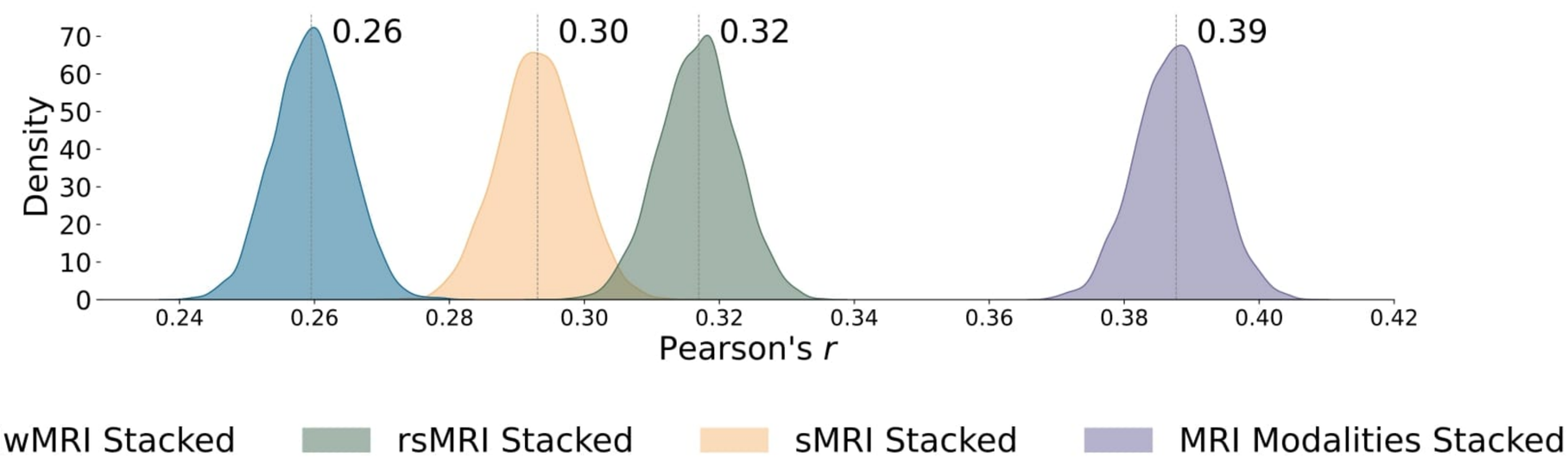

b

Bootstrap Distribution of Pearson's *r*: PLSR

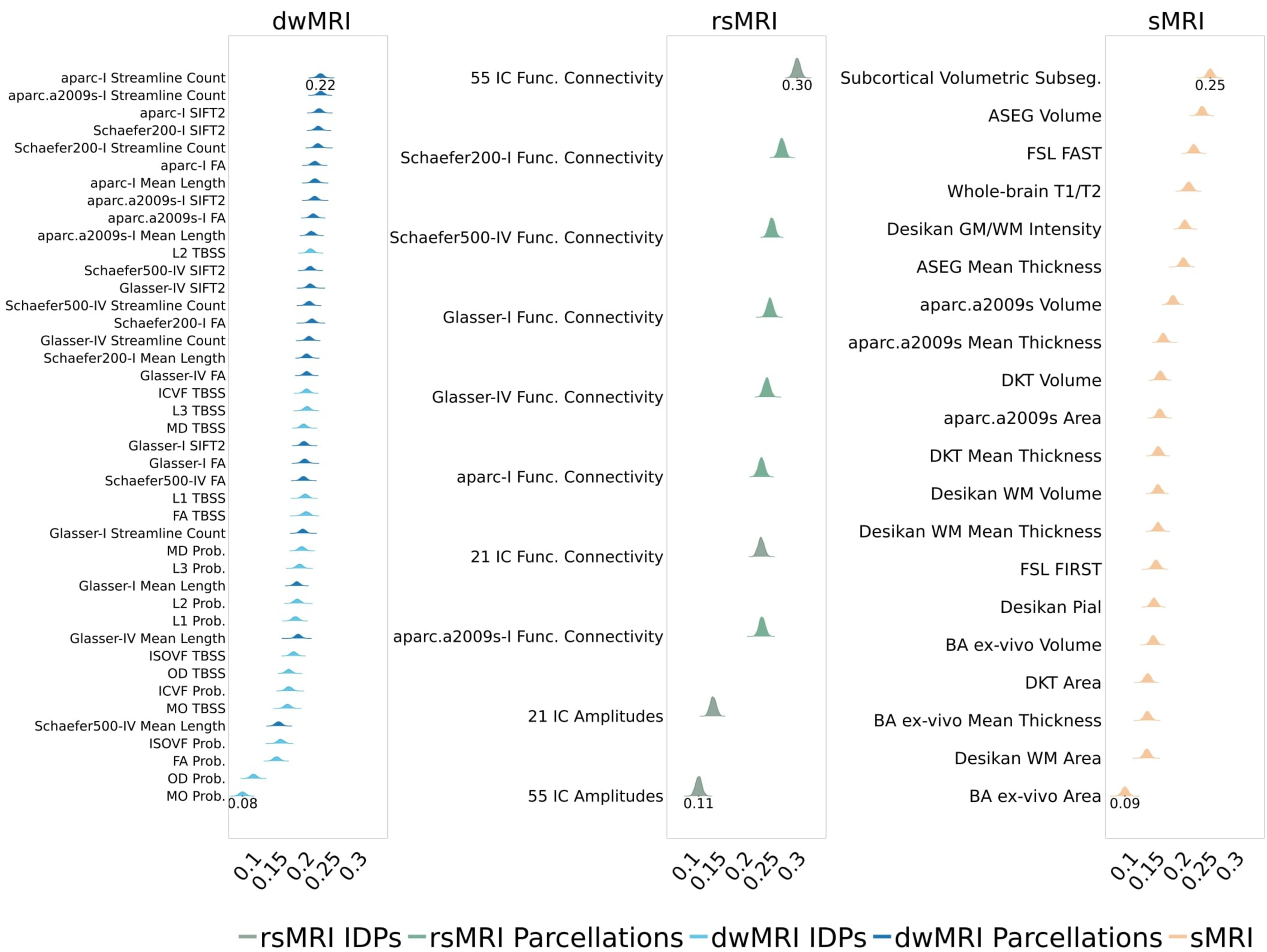

a

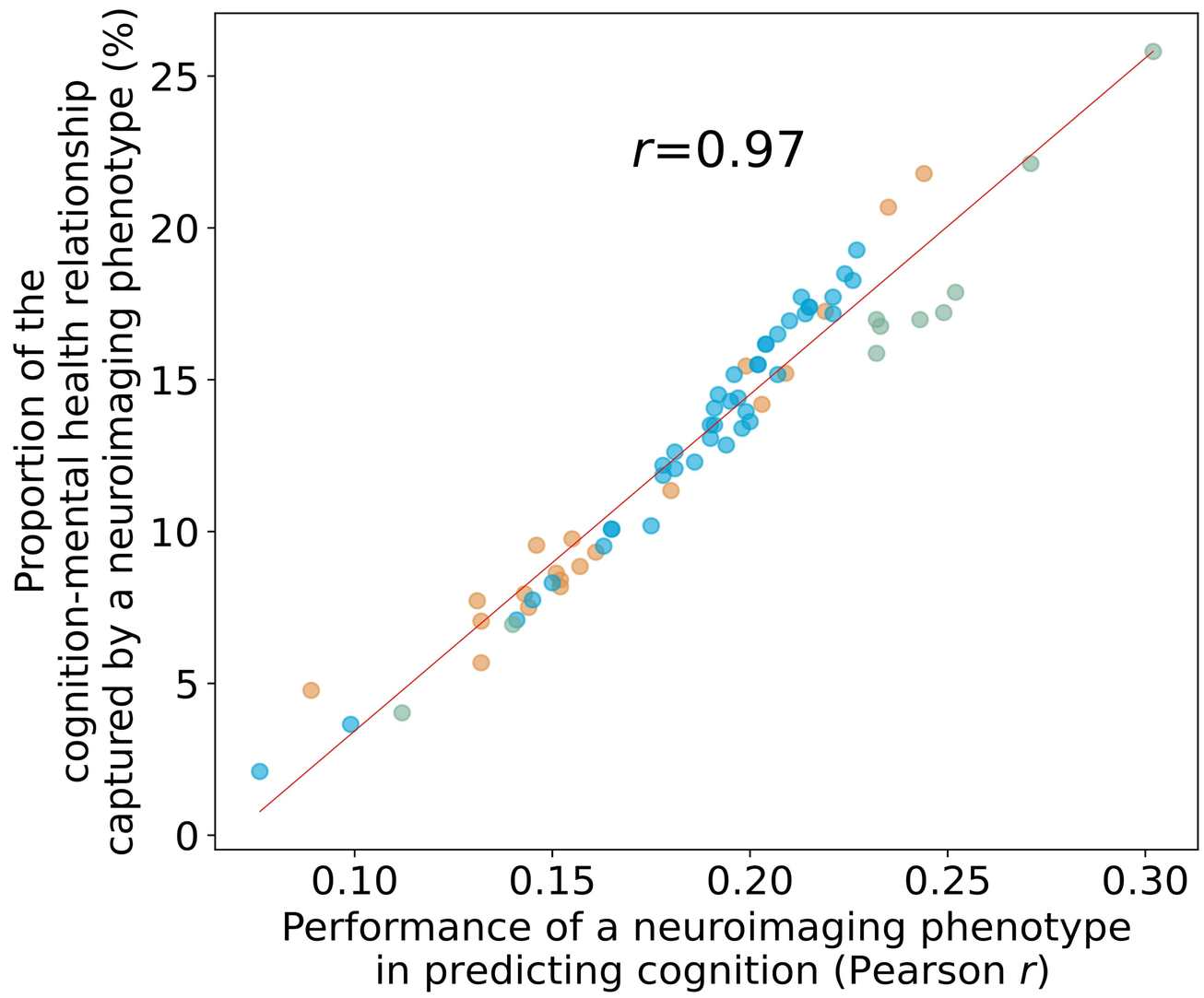
r=0.97
Proportion of the cognition-mental health relationship captured by a neuroimaging phenotype (%)
Performance of a neuroimaging phenotype in predicting cognition (Pearson r)
0
5
10
15
20
25
0.10
0.15
0.20
0.25
0.30

b

dwMRI
aparc.a2009s-I Streamline Count 7.3% 1.7% 3.3%
Schaefer200-I SIFT2 7.4% 1.6% 3.3%
Schaefer200-I Streamline Count 7.5% 1.5% 3.3%
aparc-I Streamline Count 7.4% 1.6% 3.3%
aparc-I Mean Length 7.5% 1.6% 3.2%
aparc-I SIFT2 7.4% 1.7% 3.1%
Schaefer200-I FA 7.5% 1.5% 3.1%
aparc.a2009s-I SIFT2 7.5% 1.6% 3.0%
aparc.a2009s-I FA 7.4% 1.6% 3.0%
aparc-I FA 7.5% 1.5% 3.0%
Schaefer500-IV SIFT2 7.6% 1.5% 2.9%
L2 TBSS 7.7% 1.4% 2.9%
Glasser-IV SIFT2 7.6% 1.5% 2.9%
Schaefer500-IV Streamline Count 7.6% 1.4% 2.9%
Glasser-IV Streamline Count 7.6% 1.4% 2.9%
Glasser-IV FA 7.7% 1.3% 2.9%
aparc.a2009s-I Mean Length 7.5% 1.5% 2.9%
Schaefer500-IV FA 7.8% 1.2% 2.8%
Glasser-I FA 7.8% 1.2% 2.7%
L1 TBSS 7.7% 1.3% 2.7%
FA TBSS 7.8% 1.2% 2.7%
L3 TBSS 7.8% 1.2% 2.7%
MD TBSS 7.9% 1.2% 2.7%
Schaefer200-I Mean Length 7.7% 1.4% 2.7%
Glasser-I SIFT2 7.7% 1.3% 2.6%
Glasser-I Streamline Count 7.8% 1.3% 2.6%
ICVF TBSS 7.8% 1.3% 2.5%
MD Prob. 7.8% 1.2% 2.5%
Glasser-IV Mean Length 7.9% 1.1% 2.4%
Glasser-I Mean Length 7.9% 1.1% 2.4%
L3 Prob. 7.9% 1.1% 2.3%
L2 Prob. 7.9% 1.1% 2.2%
ISOVF TBSS 8.1% 0.9% 2.1%
L1 Prob. 8.0% 1.1% 2.1%
ICVF Prob. 8.1% 0.9% 1.9%
OD TBSS 8.1% 0.9% 1.7%
MO TBSS 8.2% 0.9% 1.7%
Schaefer500-IV Mean Length 8.3% 0.7% 1.5%
ISOVF Prob. 8.3% 0.7% 1.5%
FA Prob. 8.4% 0.6% 1.5%
OD Prob. 8.7% 0.3% 0.5%
MO Prob. 8.8% 0.2% 0.4%
0 2 4 6 8 10 12
rsMRI
55 IC Func. Connectivity 6.6% 2.3% 5.8%
Schaefer200-I Func. Connectivity 7.0% 2.0% 4.8%
Schaefer500-IV Func. Connectivity 7.3% 1.6% 4.4%
Glasser-I Func. Connectivity 7.4% 1.5% 4.1%
Glasser-IV Func. Connectivity 7.4% 1.5% 3.9%
21 IC Func. Connectivity 7.5% 1.4% 3.5%
aparc.a2009s-I Func. Connectivity 7.5% 1.5% 3.5%
aparc-I Func. Connectivity 7.4% 1.5% 3.3%
55 IC Amplitudes 8.3% 0.6% 1.3%
21 IC Amplitudes 8.6% 0.4% 0.8%
0 2 4 6 8 10 12 14
sMRI
Subcortical Volumetric Subseg. 6.9% 1.9% 4.2%
ASEG Volume 7.0% 1.8% 4.0%
FSL FAST 7.3% 1.5% 3.4%
Whole-brain T1/T2 7.5% 1.3% 3.2%
Desikan GM/WM Intensity 7.6% 1.2% 2.6%
ASEG Mean Thickness 7.4% 1.4% 2.6%
aparc.a2009s Volume 7.8% 1.0% 2.2%
aparc.a2009s Mean Thickness 8.0% 0.8% 1.6%
FSL FIRST 8.0% 0.8% 1.6%
aparc.a2009s Area 8.0% 0.9% 1.6%
DKT Volume 8.0% 0.8% 1.6%
Desikan WM Volume 8.1% 0.7% 1.5%
BA ex-vivo Volume 8.1% 0.7% 1.5%
Desikan WM Mean Thickness 8.1% 0.8% 1.4%
DKT Mean Thickness 8.1% 0.7% 1.4%
Desikan Pial 8.1% 0.7% 1.4%
DKT Area 8.2% 0.6% 1.1%
Desikan WM Area 8.1% 0.7% 1.1%
BA ex-vivo Mean Thickness 8.3% 0.5% 1.0%
BA ex-vivo Area 8.4% 0.4% 0.7%
0 2 4 6 8 10 12
% Variance Explained
Common Variance: Mental Health + dwMRI
Common Variance: Mental Health + rsMRI
Common Variance: Mental Health + sMRI
Unique variance: Mental Health
Unique variance: dwMRI
Unique variance: rsMRI
Unique variance: sMRI

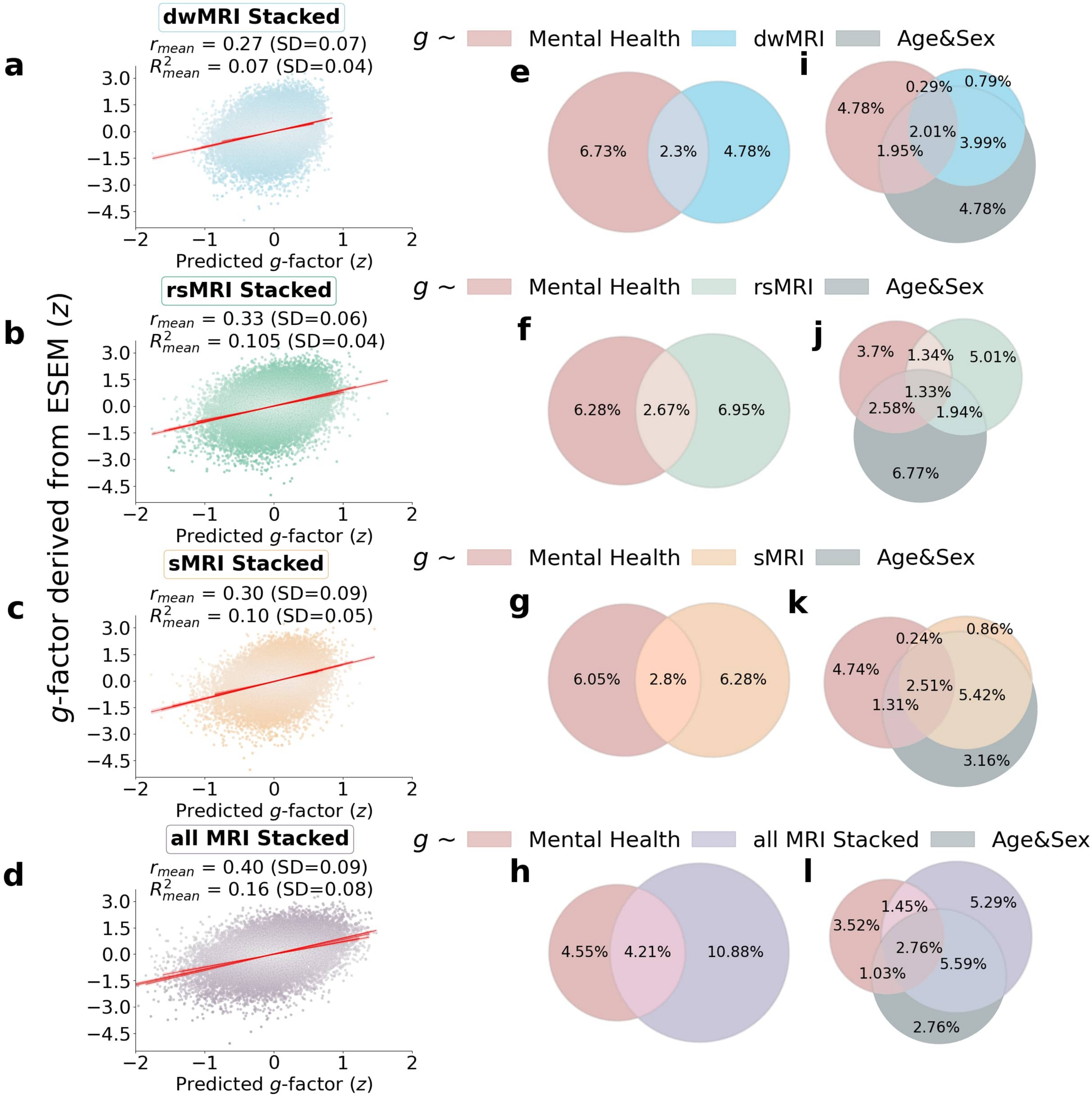
a
dwMRI Stacked
r_{mean} = 0.27 (SD=0.07)
R^2_{mean} = 0.07 (SD=0.04)
Predicted g-factor (z)
g ~ Mental Health dwMRI Age&Sex
e
6.73% 2.3% 4.78%
i
0.29% 0.79% 4.78% 2.01% 3.99% 1.95% 4.78%
b
rsMRI Stacked
r_{mean} = 0.33 (SD=0.06)
R^2_{mean} = 0.105 (SD=0.04)
Predicted g-factor (z)
g ~ Mental Health rsMRI Age&Sex
f
6.28% 2.67% 6.95%
j
3.7% 1.34% 5.01% 1.33% 2.58% 1.94% 6.77%
c
sMRI Stacked
r_{mean} = 0.30 (SD=0.09)
R^2_{mean} = 0.10 (SD=0.05)
Predicted g-factor (z)
g ~ Mental Health sMRI Age&Sex
g
6.05% 2.8% 6.28%
k
0.24% 0.86% 4.74% 2.51% 5.42% 1.31% 3.16%
d
all MRI Stacked
r_{mean} = 0.40 (SD=0.09)
R^2_{mean} = 0.16 (SD=0.08)
Predicted g-factor (z)
g ~ Mental Health all MRI Stacked Age&Sex
h
4.55% 4.21% 10.88%
l
1.45% 5.29% 3.52% 2.76% 5.59% 1.03% 2.76%
g-factor derived from ESEM (z)